HHS Public Access

Author manuscript

Sens Actuators B Chem. Author manuscript; available in PMC 2021 March 01.

Published in final edited form as:

Sens Actuators B Chem. 2020 March 1; 306: . doi:10.1016/j.snb.2019.127446.

An Activatable NIR Fluorescent Rosol for Selectively Imaging Nitroreductase Activity

Jessica L. Klockow[1,†], **Kenneth S. Hettie**[1,†,*], **Edward L. LaGory**[2], **Eui Jung Moon**[2], **Amato J. Giaccia**[2], **Edward E. Graves**[1,2], **Frederick T. Chin**[1,*]

[1]Department of Radiology, Stanford University, Stanford, CA, 94305, USA

[2]Department of Radiation Oncology, Stanford University, Stanford, CA, 94305, USA

Abstract

Hypoxia ($pO_2 \leq$ ~1.5%) is an important characteristic of tumor microenvironments that directly correlates with resistance against first-line therapies and tumor proliferation/infiltration. The ability to accurately identify hypoxic tumor cells/tissue could afford tailored therapeutic regimens for personalized treatment, development of more-effective therapies, and discerning the mechanisms underlying disease progression. Fluorogenic constructs identifying aforesaid cells/tissue operate by targeting the bioreductive activity of primarily nitroreductases (NTRs), but collectively present photophysical and/or physicochemical shortcomings that could limit effectiveness. To overcome these limitations, we present the rational design, development, and evaluation of the first activatable ultracompact xanthene core-based molecular probe (**NO_2-Rosol**) for selectively imaging NTR activity that affords an "OFF-ON" near-infrared (NIR) fluorescence response (> 700 nm) alongside a remarkable Stokes shift (> 150 nm) via NTR activity-facilitated modulation to its energetics whose resultant interplay discontinues an intramolecular d-PET fluorescence-quenching mechanism transpiring between directly-linked electronically-uncoupled **π**-systems comprising its components. DFT calculations guided selection of a suitable fluorogenic scaffold and nitroaromatic moiety candidate that when adjoined could (i) afford such photophysical response upon bioreduction by upregulated NTR activity in hypoxic tumor cells/tissue and (ii) employ a retention mechanism strategy that capitalizes on an inherent physical

[*]Corresponding author: Kenneth S. Hettie, Ph.D., 3165 Porter Drive, Palo Alto, CA 94304, khettie@stanford.edu, Frederick T. Chin, Ph.D., 3165 Porter Drive, Room 2129, Palo Alto, CA 94304, chinf@stanford.edu.

Author Contributions

Project conceptualized, designed, and managed by KSH; **NO_2-Rosol** designed and synthesized by KSH; experiments designed by KSH, JLK, and FTC; hypoxia experiments designed by JLK, KSH, and EEG; LC-MS reaction experiments performed by ELL; data acquired by JLK, KSH, ELL, and EJM; data analyzed by KSH, JLK, ELL, and EJM; an initial draft of the manuscript was prepared by JLK; any and all subsequent complete overhauled drafts, including the final draft of the manuscript, were entirely written by KSH; the final manuscript was reviewed by all parties.

[†]Co-first author (the co-first authors are listed in arbitrary order)

[†]Equal contribution

Competing Interests

The authors declare that they have no competing interests.

Declaration of interests

The authors declare that they have no known competing financial interests or personal relationships that could have appeared to influence the work reported in this paper.

property of the NIR fluorogenic scaffold for achieving signal amplification. **NO_2-Rosol** demonstrated 705 nm NIR fluorescence emission and 157 nm Stokes shift, selectivity for NTR over relevant bioanalytes, and a 28-/12-fold fluorescence enhancement in solution and between cells cultured under different oxic conditions, respectively. In establishing feasibility for **NO_2-Rosol** to provide favorable contrast levels in *solutio*/*vitro*, we anticipate **NO_2-Rosol** doing so in preclinical studies.

Graphical Abstract

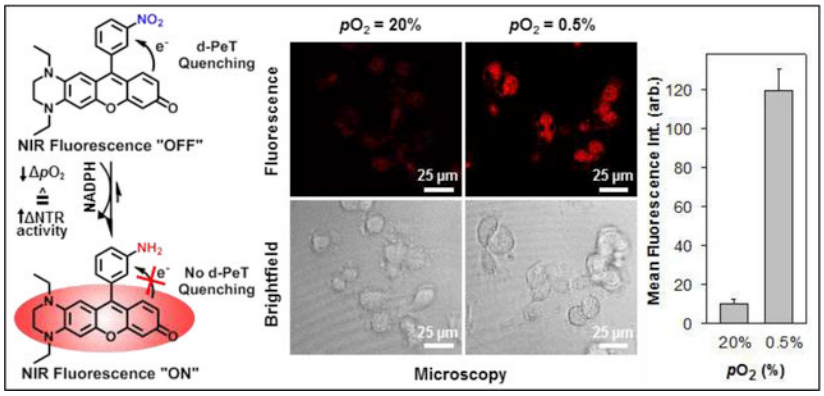

Keywords

hypoxia; fluorescence; imaging; nitroreductase; activatable probe; near-infrared

1. Introduction

Hypoxia in tumor tissue (i.e., $pO_2 \leq$ ~1.5%) results in such tissue presenting more aggressive and invasive phenotypes compared to well-oxygenated tumor tissue.[1] Tumor hypoxia is associated with reduced apoptosis, increased resistance to chemotherapy, greater metastatic potential, genomic instability, and upregulation of several stem cell genes.[2] Fluorogenic constructs that can allow for accurately identifying hypoxic tumor cells/tissue could (i) enhance current standard of care via affording the tailoring of therapeutic regimens for personalized treatment, (ii) advance the development of more-effective therapeutic agents for treating said diseased tissue, and (iii) aid basic science research efforts that strive to understand the mechanisms by which tumors spread and evade therapies.

The traditional technique (“gold standard”) employed for assessing the oxygenation level(s) in tumor tissue entails the use of an oxygen microelectrode that allows for *in vivo* measurement of dissolved oxygen.[3] In doing so, this technique requires that the microelectrode penetrate into the tumor tissue which is considered *ipso facto* as an invasive technique. For noninvasively assessing the level of hypoxia in tumor tissue, *non-optical* and *optical* imaging techniques can be utilized for such purpose.[4–7] *Non-optical* imaging techniques such as magnetic resonance imaging (e.g., BOLD-MRI) and positron emission tomography (PET) are the mainstays of current standard of care for identifying hypoxic tumor tissue, but suffer the drawback of misreporting on the actual oxygenation levels in

tumor tissue by relaying information on the *blood* oxygenation level within its vasculature and employing radiolabeled molecular imaging agents (e.g., ^{18}F-FDG, ^{18}F-MISO, ^{64}Cu-ATSM, and etc.) that afford notably poor contrast levels (i.e., tumor-to-background ratios) in conjunction with potentially significant exposure to radiation, respectively.[8–10] *Optical* imaging techniques, namely fluorescence imaging, offer a compelling approach for assessing low-oxygen levels within tumor tissue due to their ability to afford high sensitivity, high spatiotemporal resolution, simple implementation, multiplexing capabilities, and real-time imaging as well as avoiding the drawback(s) of the aforesaid non-optical imaging techniques.[11]

The literature is replete with examples of constructs that have been designed for the fluorescence imaging of hypoxia in cells/tissue, which primarily include (i) nanoprobes,[12] (ii) cationic conjugated polymers,[13] (iii) small-molecule probes utilizing *multi*-photon excitation,[14] and (iv) the small-molecule probes that employ *single*-photon excitation.[15–18] The vast majority of constructs developed for the purpose of imaging hypoxic tumor tissue rely on, in part, an internal charge transfer (ICT), Förster resonance energy transfer (FRET), or an acceptor-/donor-excited photoinduced electron transfer (a-/d-PeT) mechanism to afford their incorporated fluorogenic scaffold an OFF-ON fluorescence response via bioreductive activation primarily by either azoreductase, DT-diaphorase, or other nitroreductase (NTRs), wherein which specific said enzyme that is targeted is contingent upon which particular class of functionalized moiety is incorporated into the construct as such to serve as the recognition element for the enzyme.

The preponderance of fluorogenic constructs that utilize an ICT mechanism to operate for the aforesaid purpose typically involve a recognition element towards an aforesaid enzyme that also functions as a self-immolative linker to implement an enzymatic-triggered uncaging of the fluorogenic scaffold of said construct via an elimination process that results in said linker permanently departing from the initial form of the fluorogenic construct to afford ICT across its donor-acceptor π-system upon such bioreductive activation, and thereby the inclusion of said linker could adversely affect its efficacy by imparting an unfavorable net charge, size, and/or mass to it as so to impair its diffusion or extravasation into hypoxic tumor tissue. Moreover, the use of an ICT mechanism for such purpose could afford only a limited suppression to its spectral profile that corresponds to the fluorescence response “OFF” state of a given fluorogenic construct. Accordingly, any such dampening afforded to the spectral profile of a fluorogenic construct via employing an ICT mechanism could result in providing limited enhancements between its fluorescence response “OFF” and “ON” state due to promoting an elevated background.

Nearly all fluorogenic constructs employing a FRET or PeT mechanism for indirectly reporting on the oxygenation levels of tumor tissue via the bioreductive activity of an aforesaid enzyme entail the use of a tethering (i.e., not directly linked) fluorescence-quenching entity not directly bearing or directly bearing the recognition element for said enzyme that is relatively large or small in size/mass as well as relatively distant or proximal to the fluorogenic scaffold of such construct, respectively. For these FRET- or PeT-operating fluorogenic constructs, the bioreductive activity of an aforesaid enzyme towards the functional group of the particular corresponding recognition element that said enzyme

interacts with results in transforming said functional group such that (i) the tether itself is severed so as to eliminate the fluorescence-quenching entity from said construct or (ii) the energetics of the fluorescence-quenching entity are modulated such that their interplay between the fluorogenic construct and said fluorescence-quenching entity is modulated, respectively, and thereby the fluorogenic scaffold of the construct transitions from a fluorescence response “OFF” to “ON” state. Similar to the potential negative impact that a self-immolative linker could have on an ICT-operating fluorogenic construct, the inclusion of an aforesaid tethering fluorescence-quenching entity that is appended to a FRET- or PeT-operating fluorogenic construct could adversely affect its diffusion or extravasation into hypoxic tumor tissue by also imparting an unfavorable net charge, size, and/or mass to it.

Regardless of the particular mechanism by which any given fluorogenic construct operates to relay information on the oxygenation levels of tumor tissue, nearly all of the fluorogenic scaffolds that are a component of such constructs developed for said purpose do not display a fluorescence emission wavelength that is within the near-infrared (NIR) optical imaging window (ca. 700 – 900 nm). As a result, the use of a fluorogenic scaffold that affords a non-NIR fluorescence emission wavelength greatly hampers the ability of its construct to provide for the accurate identification of hypoxic tumor tissue due to its limited ability to provide for the visualization of deeply-embedded hypoxic tumor tissue. Virtually all of the limited number of constructs that do consist of, in part, a fluorogenic scaffold capable of affording a NIR fluorescence emission wavelength upon their bioreductive activation via an aforesaid enzyme primarily employ a dicarbocyanine or Changsha core-based structure as its fluorogenic scaffold, both of which inherently maintain a *non-neutral* net charge and are of a large size (relative to almost all other fluorogenic core structures). Moreover, both the aforesaid scaffolds and those affording a non-NIR fluorescence emission wavelength also maintain a small-to-moderate Stokes shift (ca. 10 – 100 nm), and thereby could similarly impede the ability of its fluorogenic construct to aid in the identification of deeply-embedded hypoxic tumor tissue due to catering towards allowing for an elevated instrumentation source background.

All things considered, these current fluorogenic constructs collectively suffer from the photophysical and/or physicochemical shortcomings of (i) exhibiting visible wavelength fluorescence emission (ca. 390 – 700 nm) which affords limited penetration depth in tissue, (ii) demonstrating a relatively small Stokes shift (ca. < 100 nm) which could reduce detection sensitivity due to promoting an elevated instrumentation source background, (iii) not employing an effective retention mechanism strategy which could reduce contrast levels due to affording a weak signal, (iv) maintaining an initial/inherent net charge which could hinder their delivery into hypoxic tumor tissue (as opposed to the interstitium) by impeding their diffusion across the *cell membrane* or their extravasation (diffusion/convection) from the blood across *intact microvascular walls*, (v) consisting of an effective diameter greater than ~2.0 nm or a relative molecular mass (M_r) of greater than ~15,000 which could similarly restrict their delivery into hypoxic tumor tissue,[20] and/or (vi) requiring instrumentation that is not widely available in the preclinical and/or clinical setting (e.g., two-photon fluorescence imaging instrumentation).

Of the aforesaid enzymes, the majority of fluorogenic constructs that have been developed as so to aid in discriminating between hypoxic and normoxic tumor cells/tissue using fluorescence imaging have primarily targeted NTR, presumably due to NTR demonstrating a positive correlation between its activity and the degree of hypoxia in tumor tissue. NTR is a member of the superfamily of flavin-dependent enzymes which selectively demonstrates bioreductive activity towards the nitro group of nitroaromatic moieties when in the presence of nicotinamide adenine dinucleotide phosphate (NADPH) as a cofactor (reducing agent).[21–23] NTR activity facilitates in the reduction of the nitro group of nitroaromatics to the corresponding amine group via producing a nitrosoaromatic intermediate (i.e., O_2N-aromatic → ON-aromatic). Importantly, NTRs have been shown to be upregulated in pancreatic,[24] liver,[25] colorectal,[26] osteosarcoma,[27] lung,[28] breast,[29] ovarian,[30] and cervical[31] cancers with higher expression generally correlating with poorer prognosis.[32] In addition, there is evidence that NAD(P)H:quinone oxidoreductase 1 (NQO1), a two-electron transfer "Type I" NTR, binds to and stabilizes hypoxia inducible factor 1 alpha (HIF-1α) which triggers the downstream production of pro-tumor oncogenes.[32] As shown in Figure 1, Type I and Type II NTRs facilitate the reduction of nitroaromatics through an oxygen-*insensitive* and oxygen-*sensitive* process via of a two-electron and successive one-electron transfer process, respectively, in producing the nitrosoaromatic intermediate. It is well-established that low-oxygen (low pO_2) cellular conditions elicit and upregulate the bioreductive activity of Type II NTRs, wherein the suppressed back-reaction of its futile redox cycle largely restricts re-oxidation of the nitro radical anion intermediate such that regeneration of the parent nitroaromatic is predominantly inhibited.

To overcome the collective shortcomings of fluorogenic constructs currently developed for assessing the oxygenation levels in tumor tissue, we conceived of a fluorogenic construct that could, in part, exploit the upregulated NTR activity that is elicited from tumor tissue when under low-oxygen conditions as such that it affords both negligible background autofluorescence *and* minimal instrumentation source background, yet importantly, we concurrently imagined we could fashion it as so to also afford effective signal amplification. Moreover, we also envisioned for the aforesaid fluorogenic construct that it could be well-suited for delivery into hypoxic tumor tissue by tailoring it as so to maintain a neutral net charge and small effective diameter (i.e., < 2 nm) for unrestricted (i) diffusion across the *cell membrane* and (ii) extravasation (diffusion/convection) from the blood across *intact microvascular walls*. By doing so, we were able to subsequently lay out an ultracompact uncharged NIR fluorogenic construct for selectively imaging nitroreductase activity that could afford enhanced contrast levels, in part, via a combination of exhibiting (i) negligible background autofluorescence, (ii) minimal instrumentation source background, and (iii) effective signal amplification, all to aid in the accurate identification of hypoxic tumor tissue upon its potential future translation into relevant *in vivo* applications.

Herein, we provide the rational design, development, and feasibility studies of **NO_2-Rosol**, the first activatable ultracompact xanthene core-based molecular probe for selectively imaging NTR activity as so to demonstrate an "OFF-ON" NIR fluorescence response (i.e., > 700 nm) alongside a remarkable Stokes shift (i.e., > 100 nm) afforded via a modulation to the interplay of the energetics initially enabling an intramolecular donor-excited

photoinduced electron transfer (d-PeT) fluorescence-quenching process to transpire between the directly-linked electronically-uncoupled π-system of its (i) NIR fluorogenic scaffold and (ii) pendant nitroaromatic moiety components upon NTR activity-facilitated complete reduction of the nitro group of said moiety to the corresponding amine group such that the transformation imparts to its components aptly-situated energetics whose resultant interplay results in relieving (dequenching) the suppressed NIR fluorescence response from the NIR fluorogenic scaffold by precluding the aforesaid d-PeT fluorescence-quenching process from occurring. **NO_2-Rosol** was prepared with, in part, the aid of density functional theory (DFT) calculations to efficiently identify a suitable fluorogenic scaffold and nitroaromatic moiety candidate that when adjoined would comprise a molecular probe capable of providing enhanced contrast levels via (i) affording the aforesaid photophysical response through aforesaid mechanism alongside a noteworthy Stokes shift both upon its bioreductive activation facilitated by and for exploiting upregulated NTR activity elicited from hypoxic tumor tissue and (ii) employing an effective retention mechanism strategy that operates by leveraging an inherent physical property of the NIR fluorogenic scaffold to afford signal amplification. **NO_2-Rosol** demonstrated 705 nm NIR fluorescence emission and a 157 nm Stokes shift upon NTR activity-facilitated bioreductive activation, selectivity for NTR over relevant bioanalytes, and a 28-/12-fold fluorescence enhancement in solution and between cells cultured under normoxic and hypoxic conditions, respectively. In establishing feasibility for **NO_2-Rosol** to afford enhanced contrast levels *in solutio* and *in vitro*, we anticipate **NO_2-Rosol** similarly doing so upon pursuing preclinical studies. Taken together, **NO_2-Rosol** serves as a proof-of-concept for the effective fashioning and implementation of an activatable ultracompact xanthene core-based NIR fluorogenic molecular probe tailored towards selectively imaging NTR activity using rational design.

We harnessed the use of DFT calculations to facilitate the rational design of **NO_2-Rosol**, wherein they guided our design and selection of (i) a fluorogenic scaffold amongst other scaffold candidates and (ii) an appended nitroaromatic moiety that we believed could afford the proposed fluorogenic molecular probe an OFF-ON NIR fluorescence response in conjunction with a remarkable Stokes shift, both of which are simultaneously afforded by and initiate via a modulation to a d-PeT process governing its fluorescence response “OFF” to “ON” state. On doing so, we were able to select a highly-specific combination of components with well-situated energetics that we believed could serve our intended purpose. Incidentally, we arrived at pairing a xanthene core-based fluorogenic scaffold that is identical to that which underlies THQ-Rosol with a pendant *m*-nitrobenzene that we situated at its 9’-position. In doing so, we believed the *m*-nitrobenzene recognition element would have a π-system that would be essentially orthogonal to that of the aforesaid fluorogenic scaffold similar to that of analogously-configured molecular platforms including rhodamine-, rhodol-,[34] coumarin-3-aldehyde-,[35–37] and BODIPY-based[12] fluorogenic constructs. As such, the separate π-system of each of the two directly-linked components would maintain limited cross-conjugation due to the minimal molecular orbital overlap that arises from their significant lack of planarity. Accordingly, we would be able to treat these two components as distinct electronically-uncoupled π-systems. We believed the particular arrangement of the molecular orbital energy levels (energetics) of the unactivated (nitro) and activated (amine) form of their pendant *m*-substituted-benzene moiety in relation to those of

the fluorogenic scaffold would impart an OFF-ON NIR fluorescence response to **NO_2-Rosol** upon the nitro group of the *m*-nitrobenzene undergoing complete reduction to the corresponding amine group facilitated by upregulated NTR activity that is elicited from hypoxic tissue. Accordingly, we envisaged **NO_2-Rosol** would be an activatable analogue of THQ-Rosol that would demonstrate selectivity towards NTR activity as so to allow for the accurate identification of hypoxic tumor tissue via fluorescence imaging. Thus, **NO_2-Rosol** would be comprised of, in part, a xanthene core-based fluorogenic scaffold that integrates a 1,2,3,4-tetrahydroquinoxaline (THQ) moiety into its framework. Our earlier work demonstrated that the THQ moiety of this xanthene core-based fluorogenic scaffold imparts not only NIR fluorescence emission beyond 700 nm alongside a notable Stokes shift well beyond 100 nm to it, but the THQ moiety also imparts favorable inherent physical properties to it that could implement our retention mechanism strategy.[34,36] As we previously found THQ-Rosol to be cell-membrane permeable and retained within intracellular compartments due to the latent lysosomotropic effect upon the THQ moiety of its fluorogenic scaffold becoming weakly-protonated within select intracellular compartments. Accordingly, we believed we could also leverage this effect as a retention mechanism strategy to facilitate in obtaining enhanced contrast levels via the activated form of **NO_2-Rosol** similarly accumulating intracellularly such that it affords signal amplification.[38] On doing so, we believed (i) the complete reduction (activation) of the nitro group of its *m*-nitrobenzene to the corresponding amine group to afford *m*-aminobenzene facilitated via upregulated NTR activity and (ii) its subsequent intracellular accumulation could impart to **NO_2-Rosol** (i) selectivity towards and (ii) enhanced contrast for the fluorescence imaging of hypoxic tumor tissue.

In all, we envisaged the operational process for achieving enhanced contrast levels in hypoxic tumor cells/tissue(s) amongst normoxic cells/tissue(s) would occur via (i) exploiting the resultant upregulated NTR activity and suppressed back-reaction of its futile redox cycle by using an NTR-selective activatable molecular probe capable of affording an OFF-ON NIR fluorescence response upon the nitro group of its pendant nitroaromatic moiety undergoing complete reduction to the corresponding amine group facilitated by NTR activity, wherein the chemical transformation would alter the interplay of the energetics between the directly-linked electronically-uncoupled π-systems comprising its components whereby the intramolecular d-PET fluorescence-quenching process could no longer suppress the NIR fluorescence response from its fluorogenic scaffold as such that the activated form of **NO_2-Rosol** (i.e., NH_2-Rosol) represents the NIR fluorescence response “ON” state and (ii) capitalizing on a retention mechanism strategy afforded by a physical property inherent to the fluorogenic scaffold of the activated molecular probe such that it provides signal amplification via intracellular accumulation (Figure 2).

2. Results

2.1 DFT Calculations.

We performed density functional theory (DFT) calculations to obtain the highest occupied molecular orbital and lowest unoccupied molecular orbital energy values *(*E_{HOMO} and E_{LUMO}, respectively) of the fluorogenic scaffold that would underlie **NO_2-Rosol**, which

were then separately compared to those of its pendant aromatic in both the unactivated (nitro) and activated (amine) forms that we similarly calculated (Figures 3A and 3B). The calculated molecular orbital energy values revealed that the E_{LUMO} of the fluorogenic scaffold (−0.0686 hartrees) is higher in comparison to the E_{LUMO} of its pendant *m*-nitrobenzene (−0.0866 hartrees), and thereby following photoexcitation the resultant excited electron which would have originated from the HOMO of the fluorogenic scaffold and momentarily occupy the LUMO of the fluorogenic scaffold would then transfer to the LUMO of the pendant *m*-nitrobenzene due to maintaining favorable energetics for the excited electron to do so in lieu of relaxing back to the HOMO of the fluorogenic scaffold in a radiative decay process (Figure 3A). As such, this intramolecular activity between the directly-linked electronically-uncoupled π-systems would result in quenching (suppressing) the otherwise resultant fluorescence emission via a d-PeT process, wherein the excited electron that would momentarily occupy the LUMO of the *m*-nitrobenzene and subsequently relax in a non-radiative process. However, complete reduction of the nitro group of the pendant *m*-nitrobenzene to the corresponding amine group would result in the E_{LUMO} of the *m*-aminobenzene being is considerably higher (0.0118 hartrees) than the E_{LUMO} of the fluorogenic scaffold (−0.0686 hartrees), whereby following photoexcitation an intramolecular transfer of the excited electron from the LUMO of the fluorogenic scaffold to the LUMO of the *m*-aminobenzene would be energetically unfavorable (Figure 3B). Accordingly, the excited electron which would be momentarily occupying the LUMO of the fluorogenic scaffold would relax back to the HOMO of the fluorogenic scaffold in a radiative decay process as such to provide NIR fluorescence emission. Collectively, the complete reduction of the nitro group of the pendant *m*-nitrobenzene moiety of **NO_2-Rosol** to the corresponding amine group permits, upon photoexcitation, the resultant excited electron derived from the underlying fluorogenic scaffold to impart an OFF-ON NIR fluorescence response to **NO_2-Rosol** via such chemical transformation resulting in discontinuing and precluding a d-PeT fluorescence-quenching process from transpiring between its components.

2.2 Synthesis.

The molecular probe was synthesized in two steps from known starting materials (Scheme 1).[36,39,40] A Friedel-Crafts acylation of compound **1** using excess aluminum chloride as a Lewis acid successively acylates and demethylates compound **1** to directly provide compound 2 in low yield. Subsequent intermolecular cyclization with resorcinol and methanesulfonic acid yields the final product, **NO_2-Rosol**, also in low yield.

2.3 Spectroscopy.

The spectral and photophysical properties of both the unactivated (**NO_2-Rosol**) and activated (NH2-Rosol) form of the molecular probe were examined via UV-vis and fluorescence spectroscopy (Table 1.). The measured maximum absorption and maximum fluorescence emission wavelength of the unactivated form of **NO_2-Rosol** were determined to be 550 nm and 710 nm, respectively, thereby affording a significant 160 nm Stokes shift. The measured maximum absorption and fluorescence emission wavelength of the activated form of **NO_2-Rosol** were observed to be 548 nm and 705 nm, respectively, thereby affording a similarly remarkable 157 nm Stokes shift as to that of **NO_2-Rosol**. **NO_2-Rosol** and its activated form

displayed comparable molar absorptivity (ε) values of 11,000 and 10,300 $M^{-1}cm^{-1}$, respectively. We evaluated the solubility of **NO_2-Rosol** in aqueous solution throughout a range of relevant concentrations (1–30 μM) to preemptively eliminate any potential confounding factors (e.g., aggregation) that could interfere with further evaluating **NO_2-Rosol**. Accordingly, we performed a linear regression analysis by preparing a correlation plot that interrelated the resultant absorbance values of **NO_2-Rosol** (measured at 550 nm) to the corresponding concentrations of **NO_2-Rosol** that we evaluated (Figures S1A and S1B). We next performed a statistical measure between the select set of parameters and obtained the corresponding coefficient of determination (r^2) of said parameters of **NO_2-Rosol**. We calculated the r^2 value for the analyzed select set of parameters of **NO_2-Rosol** to be 0.98. As an r^2 value ≥ 0.70 corresponds to a strong relationship, the calculated r^2 value of 0.98 signified that a very strong relationship exists between the resultant absorbance values measured at 550 nm and the corresponding concentrations of **NO_2-Rosol** that we employed. As such, the r^2 value of 0.98 strongly suggests that **NO_2-Rosol** demonstrates excellent solubility in aqueous conditions throughout the range of relevant concentrations of **NO_2-Rosol** that we examined.

We initially evaluated the feasibility of **NO_2-Rosol** to undergo bioreductive activation via NTR activity via performing solution studies, wherein we determined that its activation required the presence of both NTR and the electron donor NADPH, as anticipated (Figure 4A). In doing so, **NO_2-Rosol** demonstrated a 28-fold fluorescence enhancement upon NTR activity-facilitated complete reduction to its activated form. An enzyme inhibition assay was performed by, prior to its addition to identical separate solutions containing **NO_2-Rosol** and NADPH, pretreating NTR with various concentrations of dicoumarol, which is a known inhibitor of other nitroreductases and functionally-similar NAD(P)H:quinone oxidoreductase 1 (NQO1) (Figure 4B).[41,42] As anticipated, we observed an indirect relationship between the use of an increasing concentration of dicoumarol and a correspondingly lower measured fluorescence intensity. To ensure that both forms of **NO_2-Rosol** would be suitable for fluorescence-based experiments of any extended duration of time, we evaluated the photostability of the activated and unactivated form of **NO_2-Rosol** under continuous irradiation with a 7500 mW (total output) Xenon arc lamp for 30 minutes (Figure S2). Both the unactivated (nitro) and activated (amine) forms of **NO_2-Rosol** exhibited negligible alteration to their measured fluorescence intensity throughout the selected time frame, thereby revealing that both forms of **NO_2-Rosol** demonstrate excellent photostability. Next, we evaluated the effect of altering the concentration of NTR on the fluorescence intensity of **NO_2-Rosol** (Figure 4C). On doing so, we observed correspondingly higher fluorescence intensity when using increasing concentrations of NTR.

We performed a kinetic analysis on the activation of **NO_2-Rosol** by the nitroreductase enzyme (in the presence of NADPH), wherein we set out determine the Michaelis-Menten kinetic constants by plotting corresponding experimental data according to the Lineweaver-Burk linear transformation method (Figures S3 and S4). On doing so, the activation of **NO_2-Rosol** via its NTR-catalyzed complete reduction appeared to adhere to Michaelis-Menten kinetics, and thereby we were able to calculate the values of the corresponding Michaelis

constant, K_M, and maximum of initial reaction rate, V_{max}, kinetic parameters of NTR towards activating **NO_2-Rosol** to be 4.3×10^{-6} M and 1.25×10^{-8} M/s, respectively.

To further establish that the OFF-ON NIR fluorescence response of **NO_2-Rosol** is attributable (i) to NTR activity-facilitated bioreductive activation of **NO_2-Rosol** (in the presence of NADPH) and(ii) not to the difference from a significant shift or alteration in the absorption profile between the unactivated (**NO_2-Rosol**) and activated (NH_2-Rosol) form of **NO_2-Rosol**, we obtained and compared the absorption spectrum of **NO_2-Rosol** prior to and after its reaction with NTR. (Figure 4D). The absorption profiles of **NO_2-Rosol** prior to and after reaction its reaction with NTR appeared nearly identical, wherein collectively (i) their comparable molar absorptivity and (ii) negligible difference between their maximum absorption wavelength further supported that the OFF-ON NIR fluorescence response of **NO_2-Rosol** upon interaction with NTR almost exclusively derives from the resultant 41-fold enhancement between their respective relative quantum yields upon complete reduction of **NO_2-Roosl** via NTR activity (in the presence of NADPH). Stated otherwise, as all else is essentially equal, the OFF-ON NIR fluorescence response of **NO_2-Rosol** results from the dequenching of the d-PET fluorescence-quenched **NO_2-Rosol** upon its complete reduction to NH_2-Rosol facilitated by NTR activity, all of which the resultant 41-fold enhancement between their respective relative quantum yields reflects. As other bio-/molecular probes incorporate fluorogenic scaffolds that exhibit comparable relative fluorescence quantum yields are utilized in preclinical and clinical applications, such as IRDye® 800CW (Φ_{fl} = 0.03), we presume that **NO_2-Rosol** could be similarly as effective upon its intended usage.[15,43–46]

Moreover, we detected and validated the presence of only the unactivated and activated form of **NO_2-Rosol** prior to after the reaction between NTR and **NO_2-Rosol** (in the presence of its required cofactor, NADPH), respectively, by comparing the respective distinct retention time and corresponding mass-to-charge ratio (m/z value) of each form to those of its respective synthesized standard via liquid chromatography-high resolution mass spectrometry (LC-HRMS) (Figure S5). To do so, we developed and implemented a chromatographic method with refined parameters to obtain excellent separation between the synthesized standard of the unactivated and activated form of **NO_2-Rosol**, wherein each said form of **NO_2-Rosol** maintained a retention time (t_R) of t_R = 8.2 min and t_R = 7.4 min that afforded a confirmatory corresponding m/z value of $[M+H]^+$ = 430.1768 and $[M+H]^+$ = 400.2026 as expected, respectively (Figure S5A). After doing so and as anticipated, we detected and validated the presence of the unactivated form of **NO_2-Rosol** via LC-HRMS using the aforesaid method after combining only **NO_2-Rosol** and NTR. In hopes of also accurately identifying the nitroso- and hydroxylaminoaromatic reaction intermediates to potentially glean further insight into the bioreductive reaction mechanism between **NO_2-Rosol** and NTR, we subsequently performed and quenched the reaction between **NO_2-Rosol**, NTR, and NADPH after 0.5 hr. Despite detecting and validating the presence of the unactivated and activated form at the predetermined time point based on their retention time and m/z value via LC-HRMS using the identical method, we were unable to accurately identify either aforesaid reaction intermediate species (Figure S5B).

We examined a large panel of potential competing analytes in attempts to activate **NO_2-Rosol**. Several small molecules including oxidants, reductants, amino acids, salts, and other relevant biomolecules were applied to confirm that any observed fluorescence intensity increase could only be attributed to the activation of **NO_2-Rosol** via the reductive process of NTRs (Figure 4E). Indeed, only NTR was capable of activating **NO_2-Rosol** into eliciting a significant NIR fluorescence response upon photoexcitation. We also performed a competition assay to evaluate the effect of NTR towards activating **NO_2-Rosol** when in the presence of other oxidoreductase enzymes. We noted that the resultant NIR fluorescence response of **NO_2-Rosol** neither appreciably increased nor decreased when competing enzymes were in the presence of NTR (Figure 4F). These results suggest that the observed fluorescence intensities from **NO_2-Rosol** are the result of it selectively undergoing complete reduction via nitroreductase enzymes to afford the probe in its activated form.

2.4 Cellular Analyses.

We performed Western blot analyses to determine the relative sensitivity of the cells to hypoxia before evaluating **NO_2-Rosol** *in vitro* by separating, labeling, and semi-quantifying the total expression amount of a well-known standard endogenous biomarker, carbonic anhydrase IX (CAIX), which both (i) is commonly used as a surrogate for assessing oxygenation levels in cells/tissues and (ii) positively (directly) correlates to NTR activity under both hypoxic (pO_2 = 0.5%) and normoxic (pO_2 = 20%) conditions. CAIX is a zinc metalloenzyme that catalyzes the conversion of CO_2 to bicarbonate (HCO_3^-) and H^+ in the form of the hydronium ion (H_3O^+).[47] CAIX expression level is well-known to be strongly upregulated in hypoxic tissues when compared to normoxic tissues.[48,49] We utilized two commercially-available glioblastoma (GBM) cell lines (U87 and U251) because brain cancers such as GBM are extremely prone to being in or transforming into a hypoxic state.[50] Accordingly, hypoxic conditions appeared to result in upregulating the CAIX total expression level in both cell lines, but we observed a greater increase in the CAIX total expression level of the U251 cell line in comparison to the U87 cell line (Figure 5). The second band (higher molecular weight) on the gel is reported to be the glycosylated form of expressed CAIX. Given their apparent greater sensitivity to oxygenation levels, we selected the U251 cell line for our usage in subsequent experiments. Next, we performed a viability assay to examine the toxicity of **NO_2-Rosol** at different concentration levels towards U251 cells, wherein we used Calcein-AM to stain the live cells (Figure S6). At relevant concentration levels, we observed **NO_2-Rosol** to be nontoxic towards U251 cells.

2.5 Fluorescence Microscopy.

To evaluate the ability of **NO_2-Rosol** to afford selective imaging of nitroreductase activity, we performed hypoxia experiments *in vitro* by separately applying **NO_2-Rosol** to live cells under normoxic (pO_2 = 20%) and hypoxic conditions (pO_2 = 0.5%). U251 cells were seeded onto 35 mm glass-bottom dishes and then incubated for 24 hours either in normoxic or hypoxic conditions prior to treatment with the probe. We performed confocal microscopy using the 550 nm laser line to excite **NO_2-Rosol**. As shown in Figure 6A, we obtained significantly higher fluorescence intensity from **NO_2-Rosol** when incubated with the U251 cells under hypoxic conditions (Figure 6A, right panel, pO_2 = 0.5%) than when compared to

that of those under normoxic conditions (Figure 6A, left panel, pO_2 = 20%), which further supports our hypothesis that **NO_2-Rosol** is indirectly reporting on the oxygenation levels of the cells with the apparent difference in its OFF-ON NIR fluorescence response (activation) serving as a positive reflection of upregulated bioreductive activity of NTR. Brightfield images confirmed the presence of healthy cells on the basis of their morphology (Figure 6B, lower panels). Accordingly, we attained a 12-fold increase in the mean cell fluorescence intensity from the U251 cells under hypoxic conditions when compared to that of those under normoxic conditions, which suggests that **NO_2-Rosol** appears suitable for potentially affording similarly-effective contrast levels upon use in relevant *in vivo* applications (Figure 6C).

We next sought to further examine the intracellular accumulation of **NO_2-Rosol. NO_2-Rosol** was incubated in U251 cells under hypoxic conditions and imaged using confocal fluorescence microscopy. Intracellular punctate fluorescence was observed exterior to the nucleus (Figure 7). To further investigate its localization within the cell, **NO_2-Rosol** was co-incubated with specific organelle-homing dyes and was found to overlap well with LysoTracker Green DND-26 when the separate corresponding images were overlaid. A calculated strong Pearson correlation coefficient of 0.95 validated our initial observations. As a result, it appears that the activated **NO_2-Rosol** accumulates within the cell lysosomes. We hypothesized that the THQ moiety of the fluorogenic scaffold underlying **NO_2-Rosol** afforded signal amplification upon its protonation when within, localization to, and accumulation within lysosomes.

3. Discussion

Hypoxic tumors are especially aggressive and resistant to standard therapies compared to well-oxygenated tumors. Accurate identification and visualization of hypoxic tumor cells/tissue using optical imaging techniques, such as fluorescence imaging, can facilitate further exploration of the underlying biological processes of hypoxic tumors and help stratify patients for appropriate therapy regimens. Here, we used rational design to efficiently develop **NO_2-Rosol**, the first activatable ultracompact xanthene core-based molecular probe for selectively imaging NTR activity that demonstrates an “OFF-ON” NIR fluorescence response (ca. > 700 nm) alongside a remarkable Stokes shift (ca. > 150 nm) afforded via a modulation to the interplay of the energetics initially enabling an intramolecular d-PeT fluorescence-quenching process to transpire between the directly-linked electronically-uncoupled π-system of its (i) NIR fluorogenic scaffold and (ii) pendant nitroaromatic moiety components upon NTR activity-facilitated complete reduction of the nitro group of said moiety to the corresponding amine group such that the transformation imparts to its components aptly-situated energetics whose resultant interplay results in relieving (dequenching) the suppressed NIR fluorescence response from the NIR fluorogenic scaffold by precluding the aforesaid d-PeT fluorescence-quenching process from occurring.

Though nitroreductase enzymes are constitutively and ubiquitously expressed, it is well-known that they are overexpressed in many cancers compared to healthy tissue. Low oxygenation levels are also crucial for successfully affording and sustaining the activated form of **NO_2-Rosol**, as low oxygenation levels are necessary to afford (i) the suppressed

back-reaction of its futile redox cycle as so to largely restrict re-oxidation of the nitro radical anion intermediate such that regeneration of the parent nitroaromatic is predominantly inhibited and (ii) bioreductive activation of **NO_2-Rosol** facilitated by and for it to exploit upregulated NTR activity elicited from hypoxic tumor tissue.[51–55] With further testing, fluorogenic constructs such as **NO_2-Rosol** have the potential to become the primary tools for the fluorescence imaging of hypoxic tumor tissue in preclinical and/or clinical applications due to (i) affording an activatable OFF-ON fluorescence response whose emission is within the NIR optical imaging window (ca. 700 – 900 nm), (ii) displaying a noteworthy Stokes shift (ca. > 150 nm) that minimizes instrumentation source background, (iii) employing an effective retention mechanism strategy that could provide enhanced contrast levels due to affording effective signal amplification, (iv) maintaining an inherent neutral net charge that could facilitate its delivery into hypoxic tumor cells/tissue simply via unrestricted diffusion across the *cell membrane* or its extravasation (diffusion/convection) from the blood across *intact microvascular walls*, (v) consisting of an effective diameter less than ~2.0 nm and a very small relative molecular mass (M_r) of ~430 to facilitate its delivery into hypoxic tumor tissue, and (vi) simply requiring instrumentation that is commonly deployed and available in a preclinical and/or clinical setting, collectively which current fluorogenic constructs do not demonstrate.

NO_2-Rosol is comprised of, in part, a xanthene core-based fluorogenic scaffold that integrates a THQ moiety into its framework, which has demonstrated unique photophysical and physicochemical properties when as a component of other molecular constructs, namely THQ-Rosol. Accordingly, **NO_2-Rosol** demonstrated excellent photostability in both its unactivated (nitro) and activated (amine) forms. This characteristic is particularly important for performing fluorescence microscopy studies, as typical fluorescence microscopy protocols entail cells/tissues under irradiation with a high-power laser for an extended duration of time. The ability of **NO_2-Rosol** to undergo selective bioreductive activation into a form so as to transition from a NIR fluorescence response “OFF” to “ON” state alongside demonstrating a significant Stokes shift via NTR activity, especially when under hypoxic conditions, is of particular importance for its use in *in vitro* and *in vivo* applications, as it is necessary for accurately identifying hypoxic cells/tissue with enhanced contrast levels.

Based on our analysis of the results we obtained upon performing solution studies involving competing analytes and enzymes, the ability of **NO_2-Rosol** to undergo activation and the resultant intensity of its fluorescence emission are either not or only marginally affected by the presence of other biologically-relevant molecules (Figures 4E–F). Accordingly, we attribute the fluorescence emission to the activation of **NO_2-Rosol** via nitroreductase. For its current and future potential applications, a robust signal is necessary for translating **NO_2-Rosol** into more complex biological milieu. As shown in Table 1, the drastic difference in quantum yield (41-fold) and comparable molar absorptivity values between the unactivated and activated forms of **NO_2-Rosol** when evaluated in solution further supports that the **NO_2-Rosol** is undergoing the reductive process via nitroreductase and is not merely a result of emitting fluorescence due to entering a hydrophobic pocket which includes the active site of NTR. As a transition to a less-solvated or hydrophobic environment such as the aforesaid could potentially allow for **NO_2-Rosol** to transition to NIR fluorescence response “ON”

state without the nitro group of its nitroaromatic undergoing NTR activity-facilitated complete reduction simply by such environmental effects precluding its governing d-PET fluorescence-quenching mechanism when in its NIR fluorescence "OFF" state, The similar molar absorptivity, absorbance values, and maximum absorption wavelengths of both forms of the probe (NO_2- vs. NH_2-Rosol) in solution both with and without the nitroreductase enzyme in combination with the 41-fold increase in quantum yield between the two forms of **NO_2-Rosol** further validates that the observed fluorescence emission from the probe is directly due to its activation upon undergoing bioreductive activation via NTR activity-facilitated complete reduction and not from other factors such as solvation effects (Figure 4B and Table 1).

Most noteworthy, **NO_2-Rosol** demonstrated excellent results when applied to U251 cells separately cultured under either normoxic or hypoxic conditions, wherein **NO_2-Rosol** demonstrated a 12-fold fluorescence increase in the cells cultured under hypoxic conditions when compared to that of those under normoxic conditions. The remarkable difference in fluorescence enhancement demonstrates *in solutio* and *in vitro* lays the groundwork for **NO_2-Rosol** to potentially provide similar enhanced contrast levels upon its use *in vivo*.

Cell studies demonstrate that **NO_2-Rosol** becomes trapped within the cell, which is important for signal amplification when in its activated form. **NO_2-Rosol** appears to localize and become retained within lysosomes due to the latent lysosomotropic effect, which is a common phenomenon for weak bases such as the THQ moiety of the fluorogenic scaffold underlying the **NO_2-Rosol** in both its unactivated and activated forms.[56] Accordingly, the THQ moiety has a pK_a of 5.85 when protonated, and thus the probe would assume a weakly-positive net charge upon diffusing into the acidic lysosome (pH ~5). The positive charge prevents the probe from diffusing back across the lysosomal membrane. Rather, weak-protonation of the activated **NO_2-Rosol** shifts the equilibrium gradient towards resulting in the activated **NO_2-Rosol** to accumulate within the lysosomes, which is supported by the strong punctate fluorescence we observed upon performing confocal microscopy and subsequently validated when we performed colocalization studies using LysoTracker Green DND-26.

4. Conclusion

Fluorogenic constructs that can allow for accurately identifying hypoxic tumor cells/tissue could (i) enhance current standard of care via affording the tailoring of therapeutic regimens for personalized treatment, (ii) advance the development of more-effective therapeutic agents for treating said diseased tissue, and (iii) aid basic science research efforts that aim towards understanding the mechanisms of the biological pathways that lead towards disease advancement. *Non-optical* imaging techniques such as MRI or PET suffer drawbacks that prevent or limit their ability to accurately assess the oxygenation levels within tumor tissue, respectively. *Optical* imaging techniques, namely fluorescence imaging, employ flourogenic constructs for the aforesaid purpose, yet collectively they suffer from the photophysical and/or physicochemical shortcomings of (i) exhibiting visible wavelength fluorescence emission (ca. 390 – 700 nm) which affords limited penetration depth in tissue, (ii) demonstrating a relatively small Stokes shift (ca. < 100 nm) which could reduce detection

sensitivity due to promoting an elevated instrumentation source background, (iii) not employing an effective retention mechanism strategy which could reduce contrast levels due to affording a weak signal, (iv) maintaining an initial/inherent net charge which could hinder their delivery into hypoxic tumor tissue (as opposed to the interstitium) by impeding their diffusion across the *cell membrane* or their extravasation (diffusion/convection) from the blood across *intact microvascular walls*, (v) consisting of an effective diameter greater than ~2.0 nm or a relative molecular mass (*M*r) of greater than ~15,000 which could similarly restrict their delivery into hypoxic tumor tissue, and/or (vi) requiring instrumentation that is not widely available in the preclinical and/or clinical setting (e.g., two-photon fluorescence imaging instrumentation).

To overcome these limitations for accurately identifying hypoxic tumor tissue, we have presented the rational design, development, and evaluation of the first activatable ultracompact xanthene core-based molecular probe (**NO_2-Rosol**) for selectively imaging nitroreductase (NTR) activity that affords an “OFF-ON” NIR fluorescence response alongside a remarkable Stokes shift via NTR activity-facilitated modulation to its energetics whose resultant interplay discontinues an intramolecular donor-excited photoinduced electron transfer (d-PeT) fluorescence-quenching mechanism transpiring between the directly-linked electronically-uncoupled π-systems comprising its components.

We performed and utilized DFT calculations to efficiently guide our design and selection of a suitable fluorogenic scaffold and nitroaromatic moiety candidate that when adjoined would comprise the component of **NO_2-Rosol** as such to provide enhanced contrast levels via (i) affording the aforesaid photophysical response through aforesaid mechanism alongside a noteworthy Stokes shift both upon its bioreductive activation facilitated by and for exploiting upregulated NTR activity elicited from hypoxic tumor tissue and (ii) employing an effective retention mechanism strategy that operates by leveraging an inherent physical property of the NIR fluorogenic scaffold to afford signal amplification.

NO_2-Rosol demonstrated a pronounced 705 nm NIR fluorescence emission and a 157 nm Stokes shift upon NTR activity-facilitated bioreductive activation, selectivity for NTR over relevant bioanalytes and competing enzymes, and a 28- and 12-fold fluorescence enhancement in solution and between cells cultured under different oxic conditions, respectively. In establishing feasibility for **NO_2-Rosol** to afford enhanced contrast levels *in solutio* and *in vitro* following its NTR activity-facilitated bioreductive activation upon lysosomal localization leading towards ita accumulation, we anticipate achieving similarly-desirable contrast levels upon pursuing feasibility studies with **NO_2-Rosol** in preclinical applications. Taken together, **NO_2-Rosol** serves as a proof-of-concept for the effective fashioning and implementation of an activatable ultracompact xanthene core-based NIR fluorogenic molecular probe tailored towards selectively imaging NTR activity using rational design.

5. Experimental Section

5.1 Computational methods.

DFT calculations were performed using the hybrid exchange-correlation function B3LYP with the 6–31G(d) basis set as implemented in Gaussian 09 Rev.A.02. The fluorogenic scaffold of THQ-Rosol as well as the pendant nitro- (unactivated) and aminobenzene (activated) moieties were studied *in vacuo*. Several starting geometries were used for optimization to ensure that the optimized structure corresponded to the global minimum. The final optimized geometry was unaffected by the various initial starting geometries.

5.2 Chemical synthesis.

Unless otherwise noted, all chemicals were obtained from Aldrich, Fisher, TCI America, Alfa Aesar, or Combi-Blocks and were used without further purification. Flash chromatography was performed with 32–63 mm silica gel. Ultrapure water was collected from a Milli-Q purification system.

Compound 2.—Compound **1** (366 mg, 1.13 mmol, 1 eq) was added to a small round bottom flask, dissolved in 20 mL CH_2Cl_2, wherein a stir bar was added and the flask was sealed with a rubber septum. The solution was cooled to 0°C and bubbled with N_2 gas via introducing a continuous gentle stream of N_2 gas to the solution via a needle alongside a venting needle piercing the septum. The septum was briefly lifted whilst maintaining a strong positive pressure of N_2 gas and aluminum chloride (904 mg, 6.78 mmol, 6 eq) was added quickly followed by continuous bubbling of N_2 gas. Solid 3-nitrobenzoyl chloride (230 mg, 1.24 mmol, 1.1 eq) was added in a similar fashion followed by additional bubbling of the mixture with N_2 gas. Once the solvent volume was reduced by half, the venting needle was removed maintaining a positive N_2 pressure on the flask. It was sonicated intermittently and allowed to warm to room temperature over 45 minutes. The work-up involved pouring the reaction mixture over ice and gradually basifying to ~pH 6 with a solution of saturated sodium bicarbonate. The product was extracted in a separatory funnel with CH_2Cl_2 (100 mL × 3). The organic layers were combined, dried over magnesium sulfate, and the solvent removed *in vacuo*. The crude mixture was purified via column chromatography on silica gel. The eluent consisted of 100% methylene chloride which was used to separate out impurities followed by the addition of 1–5% EtOAc to elute the product, compound 2 (80.2 mg, 0.226 mmol, 20%): ^{1}H NMR (400 MHz, $CDCl_3$) δ 12.73 (s, 1H), 8.52 (s, 1H)z, 8.36 (d, 1H, J = 7.6 Hz), 7.99 (d, 1H, J = 7.6 Hz), 7.66 (t, 1H, J = 8.0 Hz), 6.42 (s, 1H), 6.14 (s, 1H), 3.52 (t, 2H, J = 4.8 Hz), 3.43 (q, 2H, J = 7.2 Hz), 3.13 (t, 2H, J = 4.8 Hz), 3.05 (q, 2H, J = 7.2 Hz), 1.24 (t, 3H, J = 7.2 Hz), 1.06 (t, 3H, J = 7.2 Hz); ^{13}C NMR (125 MHz, $CDCl_3$) δ 193.4, 161.9, 147.9, 145.4, 141.0, 134.6, 129.5, 127.8, 125.1, 123.8, 112.3, 107.7, 96.6, 48.0, 46.0, 45.5, 45.0, 10.9, 10.1. HRMS calculated for $C_{19}H_{21}N_3O_4$ (M^+): 355.1527. Found: 355.1527.

NO_2-Rosol.—Compound 2 (147.3 mg, 0.414 mmol, 1 eq), resorcinol (45.6 mg, 0.414 mmol, 1 eq), and methane sulfonic acid (2 mL) were added to a small sealed tube and heat at 95°C overnight. The reaction mixture was poured over ice, basified to ~pH 6 with saturated sodium bicarbonate and extracted with CH_2Cl_2 (100 mL × 3). The organic fractions were combined, dried over magnesium sulfate, and the solvent reduced *in vacuo*. The crude

material was purified via column chromatography on silica gel eluting first with 100% chloroform followed by 85:15 chloroform:MeOH. **NO_2-Rosol** appeared on the column as a blue band and dried to a blue-purple solid (40.9 mg, 0.095 mmol, 23%): ^{1}H NMR (400 MHz, $CDCl_3$) δ 8.43 (d, 1H, J = 8.4 Hz), 8.27 (s, 1H), 7.79 (t, 1H, J = 8.0 Hz), 7.72 (d, 1H, *J* = 7.6 Hz), 6.91 (d, 1H, *J* = 9.6 Hz), 6.64 (dd, 1H, *J* = 1.6, 9.6 Hz), 6.60 (s, 1H), 6.56 (d, 1H, *J* = 1.6 Hz), 5.95 (s, 1H), 3.58 (t, 2H, *J* = 4.8 Hz), 3.52 (q, 2H, *J* = 7.2 Hz), 3.24 (t, 2H, *J* = 4.8 Hz), 3.06 (q, 2H, *J* = 7.2 Hz), 1.30 (t, 3H, *J* = 7.2 Hz), 0.99 Hz (t, 3H, *J* = 7.2 Hz); ^{13}C NMR (125 MHz, $CDCl_3$) δ 183.4, 158.5, 151.0, 148.3, 146.1, 143.4, 135.9, 135.5, 133.0, 129.8, 128.8, 128.2, 124.4, 124.0, 114.7, 110.9, 104.8, 104.6, 95.6, 47.6, 46.4, 45.3, 44.5, 10.7, 9.5. HRMS calculated for $C_{25}H_{24}N_3O_4$ ($M+H^+$): 430.1761. Found: 430.1759.

NH_2-Rosol.—NO_2-Rosol (38.7 mg, 0.090 mmol) was dissolved in 40 mL of EtOH and water (9:1) in a small round bottom flask with stir bar. Iron powder (70 mesh, < 212 μm, excess) was added followed by two drops of concentrated HCl. The mixture stirred and refluxed for 1 hr followed by removal of the iron with a magnet. The water/EtOH mixture was removed via rotary evaporation. The material was dissolved in a minimal amount of MeOH and transferred into a separatory funnel with water and DCM. Saturated sodium bicarbonate (50 mL) was added to the separatory funnel and the crude product was extracted into the DCM layer (50 mL × 3). The organic fractions were combined, dried over magnesium sulfate, and the solvent removed *in vacuo*. The material was purified via column chromatography on silica gel starting with 100% $CHCl_3$ eluent and ramping up polarity to 93:7 $CHCl_3$:MeOH. The product was isolated as a magenta solid (quantitative yield). ^{1}H NMR (400 MHz, $CDCl_3$) δ (ppm) 7.30 (t, 1H, *J* = 8.0 Hz), 7.18 (d, 1H, *J* = 9.6 Hz), 6.83 (ddd, 1H, *J* = 8.0 Hz, 2.4 Hz, 0.8 Hz), 6.70 (d, 1H, *J* = 7.6 Hz), 6.64–6.68 (m, 2H), 6.59 (s, 1H), 6.56 (s, 1H), 6.28 (s, 1H), 3.59 (t, 2H, *J* = 5.2 Hz), 3.51 (q, 2H, *J* = 7.2 Hz), 3.24 (t, 2H, *J* = 5.2 Hz), 3.07–3.17 (m, 2H), 1.29 (t, 3H, *J* = 7.2 Hz), 1.04 (t, 3H, *J* = 7.2 Hz); ^{13}C NMR (125 MHz, $CDCl_3$) δ (ppm) 158.7, 151.6, 151.3, 146.8, 143.8, 134.9, 133.0, 130.3, 129.5, 126.7, 119.5, 115.8, 115.8, 114.6, 112.1, 106.2, 104.2, 95.4, 47.9, 46.6, 45.6, 44.7, 29.8, 10.9, 9.7. HRMS calculated for $C_{25}H_{26}N_3O_2$ ($M+H^+$): 400.2019. Found: 400.2018.

5.3 Spectroscopy.

Absorption spectra were recorded using an Agilent 8453 UV-Visible Spectrophotometer. Fluorescence spectra were recorded using a QuantaMaster-400 (Horiba Jobin Yvon) at 37°C. Separate solutions of the **NO_2-Rosol** and NH_2-Rosol forms of the probe were prepared from a 1 mg/mL stock solution of each (in DMSO) that was diluted to volume with buffer. DMSO was added to constitute 5% of the total volume. NMR spectra were taken on an Agilent 400-MHz NMR Spectrometer. All HRMS analyses were completed using positive-ion mode electrospray ionization with an Apollo II ion source on a Bruker 12 Tesla APEX-Q FTICR-MS.

5.4 LC-HRMS.

The **NO_2-Rosol** and NH_2-Rosol standards were injected at a concentration of 1 μg/mL in methanol. The reaction mixture was allowed to react at 37°C for 30 min prior to quenching with cold methanol, lyophilizing, and resuspending in chloroform. The mixtures were centrifuged at 10,000 × g for 10 min to pellet the salts. The supernatant was saved, the

chloroform evaporated, and methanol added to achieve a final concentration of 10 μg/mL. Samples were analyzed using an Agilent 6545 Q-TOF LC/MS instrument. Compound separation was performed using a reversed phase HPLC column (Agilent Zorbax Eclipse Plus C18 2.1 × 100 mm, 1.8 μm), using an injection volume of 2.0 μL, a flow rate of 0.5 mL/min, and a gradient of mobile phase A (10 mM ammonium acetate buffer) and mobile phase B (acetonitrile). Initial mobile phase conditions (95%A, 5%B) were held for 1.5 minutes followed by a linear gradient to 100% B at 11.5 minutes. Conditions were held at 100% B until 18 minutes followed by a return to initial mobile phase conditions from 18.01–20.00 minutes. The total run time was 20 min. Positive ion mass spectra were acquired using electrospray ionization (drying temperature: 300°C; nebulizer pressure: 40 psig; drying gas flow: 11 L/min; capillary voltage (VCap): 3500 V; sheath gas temperature: 320°C; sheath gas flow: 11 L/min; nozzle voltage: 250 V; fragmentor voltage: 125 V; skimmer: 65 V; OCT 1 RF Vpp: 750 V). Extracted ion chromatograms were generated and integrated using MassHunter Qualitative Analysis software (Agilent) for the following m/z values: **NO_2-Rosol** $[M+H]^+$ = 430.1768 m/z; NH_2-Rosol $[M+H]^+$ = 400.2026 m/z.

5.5 Cell culture.

Two GBM cell lines were used for our studies. U87 cells were obtained from Dr. Sam Gambhir and U251 cells were obtained from Dr. Martin Brown, both of Stanford University. U87 cells were cultured in DMEM and U251 cells were cultured in RPMI media, each supplemented with 10% fetal bovine serum, 100 U/mL penicillin, and 100 μg/mL streptomycin. Cells were propagated at 37°C in a humidified atmosphere containing 5% CO_2 and either 0.5% or 20% O_2 depending on which experiment was being performed.

5.6 Western blot.

U87 and U251 cells were each seeded in a 100 mm culture dish and grown to ~90% confluency. Cells were placed in a hypoxia chamber (Invivo2–400; Ruskin Technologies, Leeds, United Kingdom), maintained at 0.5% oxygen for 24 hr, and then harvested by trypsinization. Cells were lysed in ice-cold Pierce RIPA buffer (Thermo Fisher, USA) containing HALT™ protease inhibitor cocktail (Thermo Fisher, USA) (~250 μL buffer for 8 million cells). After keeping on ice for 30 min and sonicating intermittently, cells were centrifuged at 14,000 rpm and 4°C for 15 min. The supernatant was saved and the pellet discarded. Protein concentration was determined by Pierce BCA Protein Assay (Thermo Fisher, USA) as recommended by the manufacturer. Samples containing 60 μg protein, NuPAGE® LDS Sample Buffer, and NuPAGE Sample Reducing Agent were heated at 70°C for 10 min to reduce the sample and then loaded into each lane of a NuPAGE 4–12% Bis-Tris protein polyacrylamide gel and were electrophoresed at 50V for 15 min then 150V for 45 min under constant voltage. Proteins were transferred to a PVDF membrane by wet blotting methods. Membranes were blocked with 5% BSA/TBST for 1 hr at room temp and incubated with antibodies against GAPDH (1:1000, ABclonal) and CAIX (1:200, Santa Cruz Biotechnology) at 4°C overnight. The secondary antibodies were incubated for 2 hr at room temp and were donkey anti-mouse polyclonal IgG conjugated with Alexa Fluor 680 (1:10,000, Abcam) or mouse anti-rabbit monoclonal IgG conjugated with CruzFluor 790 (1:10,000, Santa Cruz Biotechnology). Blots were visualized using the Odyssey infrared imaging system (LI-COR; Biosciences, Lincoln, NE). Signal intensities of each blot were

quantified using the Odyssey followed by analysis with GraphPad Prism 6 (GraphPad Software, La Jolla, CA). CAIX fluorescence intensities were normalized to the loading control, GAPDH.

5.7 Confocal microscopy.

NO_2-Rosol activation was separately examined in the U251 cell line under normoxic and hypoxic conditions using a Leica SP8 confocal fluorescence microscope. For colocalization studies, cells were plated onto 35 mm, 4-chamber glass-bottom dishes at a density of 50,000 cells/well and allowed to adhere at 37°C overnight. The cells were incubated sequentially with **NO_2-Rosol** (5 μM, 37°C, 30 min), LysoTracker Green DND-26 (5 μM, 37°C, 30 min), and Hoechst 33342 (0.5 μM, 37°C, 15 min) with one PBS wash in between each. After the final wash, cells were submerged in DMEM (without phenol red). A 40X (NA = 1.30 OIL) objective lens was used. Excitation wavelengths of λ_{ex} = 550 nm (**NO_2-Rosol**) and λ_{ex} = 504 nm (LysoTracker Green DND-26) were used. **NO_2-Rosol** emission was collected from 680–900 nm. LysoTracker Green DND-26 emission was collected from 514–530 nm. The Pearson correlation coefficient was calculated using the Fiji (ImageJ) plugin Coloc 2. For hypoxia studies, two separate batches of U251 cells were incubated at 20% O_2 and 0.5% O_2, respectively. The cells were treated with **NO_2-Rosol** (10 μM), incubated for 20 min at their respective oxygen concentrations at 37°C, then immediately transported to the microscope without performing a washing step. All instrument parameters were kept constant for both test batches. Quantitative image analysis was conducted using ImageJ software, wherein we compared whole cell mean fluorescence intensity for each test group.

5.8 Statistical analysis.

Data were expressed as the mean ± standard error of the mean (SEM) and analyzed using one-way analysis of variance, followed by Tukey *post hoc* tests from GraphPad Prism 6 (GraphPad Software, La Jolla, CA).

Supplementary Material

Refer to Web version on PubMed Central for supplementary material.

Acknowledgements

We thank Kitty Lee (Stanford Microscopy Facility) for technical assistance with cell imaging. This work was supported by the Department of Energy (DOE DE-SC0008397), The Ben and Catherine Ivy Foundation, and National Institutes of Health (NIH R21 CA205564-01A1). JLK's contribution to this work was supported in part by NIH/NCI training grant: T32 CA118681. KSH's contribution to this work was supported in part by NIH/NCI fellowship: F32 CA213620.

Biographies

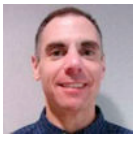

Kenneth S. Hettie, PhD

Dr. Hettie is an NIH Postdoctoral Fellow working in the Department of Radiology at Stanford University on the development and implementation of targeted probes for the visualization of cancer-related biomarkers and functional events. He specializes in rational design, chemical synthesis, and analytical evaluation of sensors and probes.

Jessica L. Klockow, PhD

Dr. Klockow is a postdoctoral scholar at Stanford University. She synthesizes and evaluates novel probes for imaging elements of the tumor microenvironment. Her areas of expertise include chemical synthesis, spectroscopic analysis and cellular assays with novel probes, the development of animal tumor models, and *in vivo* optical imaging.

Edward L. LaGory

Dr. LaGory is a postdoctoral scholar at Stanford University in the Department of Radiation Oncology. He did his doctoral work at Loyola University studying mechanisms of tumor suppression by protein kinase C. He came to Stanford in 2015. His current work involves combining molecular and cell biology approaches to elucidate mechanism and consequence of dysregulated lipid metabolism in kidney cancer.

Eui Jung Moon, PhD

Dr. Moon is a research scientist in the Department of Radiation Oncology at Stanford University and studies the effects of activation of the hypoxia inducible transcription factors (HIFs) and altered metabolic behavior in in clear cell renal cell carcinoma and other cancer types. Her areas of expertise include radiation oncology, tumor hypoxia, tumor reoxygenation, metastasis, molecular biology, DNA damage, and cell biology.

Edward E. Graves, PhD

Dr. Graves is an Associate Professor of Radiation Oncology and Radiology (by courtesy) at Stanford University who focuses on applications of emerging functional and molecular imaging techniques in radiation therapy of cancer. His research aims to identify and image *in vivo* the molecular targets that hold the most promise for targeting and monitoring response to radiation therapy. In addition, his lab displays, analyzes, and segments multiple three-dimensional datasets to generate target volumes for radiotherapy. His current interests involve the implementation and evaluation of clinical PET/CT imaging for radiation treatment planning, development and validation of novel molecular imaging methods for preclinical and clinical imaging of tumor radiosensitivity and radiation response, development of software for multimodal image analysis, and study of tumor hypoxia and radioresistance in small animal models using a multimodality molecular imaging approach.

Frederick T. Chin, PhD

Dr. Chin is an Assistant Professor of Radiology at Stanford University with nearly 22 years of experience in the field of radiopharmaceutical and tracer development for molecular imaging. He completed an NIH postdoctoral fellow in the National Institute of Mental Health where he made and developed many radiopharmaceuticals that were used to study neuropsychiatric-related disorders such stress, anxiety and Parkinson's disease. His research areas of interest include developing new strategies for: 1) novel radioligand and radiotracer development for various targets involved in brain and cancer biology, 2) radiolabeling methods of small molecules, peptides, and antibodies, and 3) clinical translation of useful radiopharmaceuticals for early-detection of disease and monitoring therapy.

References

(1). Carreau A; Hafny-Rahbi BE; Matejuk A; Grillon C; Kieda C Why Is the Partial Oxygen Pressure of Human Tissues a Crucial Parameter? Small Molecules and Hypoxia. J Cell Mol Med 2011, 15 (6), 1239–1253. 10.1111/j.1582-4934.2011.01258.x. [PubMed: 21251211]

(2). Yun Z; Lin Q Hypoxia and Regulation of Cancer Cell Stemness In Tumor Microenvironment and Cellular Stress; Advances in Experimental Medicine and Biology; Springer, New York, NY, 2014; pp 41–53. 10.1007/978-1-4614-5915-6_2.

(3). Olive Peggy L., A.-P. C, Banáth Judit P. Measuring Hypoxia in Solid Tumours&Is There a Gold Standard? Acta Oncologica 2001, 40 (8), 917–923. 10.1080/02841860152708189. [PubMed: 11845955]

(4). Lopci E; Grassi I; Chiti A; Nanni C; Cicoria G; Toschi L; Fonti C; Lodi F; Mattioli S; Fanti S PET Radiopharmaceuticals for Imaging of Tumor Hypoxia: A Review of the Evidence. American Journal of Nuclear Medicine and Molecular Imaging 2014, 4 (4), 365–384. [PubMed: 24982822]

(5). Krohn KA; Link JM; Mason RP Molecular Imaging of Hypoxia. J Nucl Med 2008, 49 (Suppl 2), 129S–148S. 10.2967/jnumed.107.045914. [PubMed: 18523070]

(6). O'Connor J; Robinson S; Waterton J Imaging Tumour Hypoxia with Oxygen-Enhanced MRI and BOLD MRI. Br J Radiol 2018, 20180642 10.1259/bjr.20180642.

(7). Sandhu S; Kydd L; Jaworski J Luminescent Probe Based Techniques for Hypoxia Imaging. J Nanomed Res 2017, 6 (3). 10.15406/jnmr.2017.06.00160.

(8). Walsh JC; Lebedev A; Aten E; Madsen K; Marciano L; Kolb HC The Clinical Importance of Assessing Tumor Hypoxia: Relationship of Tumor Hypoxia to Prognosis and Therapeutic Opportunities. Antioxid Redox Signal 2014, 21 (10), 1516–1554. 10.1089/ars.2013.5378. [PubMed: 24512032]

(9). Kroll H; Zaharchuk G; Christen T; Heit JJ; Iv M Resting-State BOLD MRI for Perfusion and Ischemia. Top Magn Reson Imaging 2017, 26 (2), 91–96. 10.1097/RMR.0000000000000119. [PubMed: 28277456]

(10). Elmes RBP Bioreductive Fluorescent Imaging Agents: Applications to Tumour Hypoxia. Chem. Commun. (Camb.) 2016, 52 (58), 8935–8956. 10.1039/c6cc01037g. [PubMed: 26924320]

(11). James ML; Gambhir SS A Molecular Imaging Primer: Modalities, Imaging Agents, and Applications. Physiol. Rev 2012, 92 (2), 897–965. 10.1152/physrev.00049.2010. [PubMed: 22535898]

(12). Fan Y; Lu M; Yu X; He M; Zhang Y; Ma X-N; Kou J; Yu B-Y; Tian J Targeted Myocardial Hypoxia Imaging Using a Nitroreductase-Activatable Near-Infrared Fluorescent Nanoprobe. Anal. Chem 2019, 91 (10), 6585–6592. 10.1021/acs.analchem.9b00298. [PubMed: 30994329]

(13). Zhang X; Zhao Q; Li Y; Duan X; Tang Y Multifunctional Probe Based on Cationic Conjugated Polymers for Nitroreductase-Related Analysis: Sensing, Hypoxia Diagnosis, and Imaging. Anal. Chem 2017, 89 (10), 5503–5510. 10.1021/acs.analchem.7b00477. [PubMed: 28421747]

(14). Liu Y; Liu W; Li H; Yan W; Yang X; Liu D; Wang S; Zhang J Two-Photon Fluorescent Probe for Detection of Nitroreductase and Hypoxia-Specific Microenvironment of Cancer Stem Cell. Analytica Chimica Acta 2018, 1024, 177–186. 10.1016/j.aca.2018.03.030. [PubMed: 29776544]

(15). Li Y; Sun Y; Li J; Su Q; Yuan W; Dai Y; Han C; Wang Q; Feng W; Li F Ultrasensitive Near-Infrared Fluorescence-Enhanced Probe for in Vivo Nitroreductase Imaging. J. Am. Chem. Soc 2015, 137 (19), 6407–6416. 10.1021/jacs.5b04097. [PubMed: 25923361]

(16). Kiyose K; Hanaoka K; Oushiki D; Nakamura T; Kajimura M; Suematsu M; Nishimatsu H; Yamane T; Terai T; Hirata Y; et al. Hypoxia-Sensitive Fluorescent Probes for in Vivo Real-Time Fluorescence Imaging of Acute Ischemia. J. Am. Chem. Soc 2010, 132 (45), 15846–15848. 10.1021/ja105937q. [PubMed: 20979363]

(17). Zhang J; Liu H-W; Hu X-X; Li J; Liang L-H; Zhang X-B; Tan W Efficient Two-Photon Fluorescent Probe for Nitroreductase Detection and Hypoxia Imaging in Tumor Cells and Tissues. Anal. Chem 2015, 87 (23), 11832–11839. 10.1021/acs.analchem.5b03336. [PubMed: 26514276]

(18). Li Z; Li X; Gao X; Zhang Y; Shi W; Ma H Nitroreductase Detection and Hypoxic Tumor Cell Imaging by a Designed Sensitive and Selective Fluorescent Probe, 7-[(5-Nitrofuran-2-Yl)Methoxy]-3HPhenoxazin-3-One. Anal. Chem 2013, 85 (8), 3926–3932. 10.1021/ac400750r. [PubMed: 23506563]

(19). Li Y; Sun Y; Li J; Su Q; Yuan W; Dai Y; Han C; Wang Q; Feng W; Li F Ultrasensitive Near-Infrared Fluorescence-Enhanced Probe for in Vivo Nitroreductase Imaging. J. Am. Chem. Soc 2015, 137 (19), 6407–6416. 10.1021/jacs.5b04097. [PubMed: 25923361]

(20). Takakura Y; Mahato RI; Hashida M Extravasation of Macromolecules. Advanced Drug Delivery Reviews 1998, 34 (1), 93–108. 10.1016/S0169-409X(98)00006-4. [PubMed: 10837672]

(21). Mukherjee A; Rokita SE Single Amino Acid Switch between a Flavin-Dependent Dehalogenase and Nitroreductase. J. Am. Chem. Soc 2015, 137 (49), 15342–15345. 10.1021/jacs.5b07540. [PubMed: 26616824]

(22). Oliveira I. A. M. de; Bonatto D; Antonio J; Henriques P; Vargas RFG Nitroreductases: Enzymes with Environmental, Biotechnological and Clinical Importance; 2010.

(23). Nguyen-Tran H-H; Zheng G-W; Qian X-H; Xu J-H Highly Selective and Controllable Synthesis of Arylhydroxylamines by the Reduction of Nitroarenes with an Electron-Withdrawing Group Using a New Nitroreductase BaNTR1. Chem. Commun 2014, 50 (22), 2861–2864. 10.1039/C3CC48590K.

(24). Lewis AM; Ough M; Du J; Tsao M-S; Oberley LW; Cullen JJ Targeting NAD(P)H:Quinone Oxidoreductase (NQO1) in Pancreatic Cancer. Molecular Carcinogenesis 2017, 56 (7), 1825–1834. 10.1002/mc.20199. [PubMed: 28639725]

(25). Cresteil T; Jaiswal AK High Levels of Expression of the NAD(P)H:Quinone Oxidoreductase (NQO1) Gene in Tumor Cells Compared to Normal Cells of the Same Origin. Biochemical Pharmacology 1991, 42 (5), 1021–1027. 10.1016/0006-2952(91)90284-C. [PubMed: 1651729]

(26). Gibson P; Gill JH; Khan PA; Seargent JM; Martin SW; Batman PA; Griffith J; Bradley C; Double JA; Bibby MC; et al. Cytochrome P450 1B1 (CYP1B1) Is Overexpressed in Human Colon Adenocarcinomas Relative to Normal Colon: Implications for Drug Development1. Mol Cancer Ther 2003, 2 (6), 527–534. [PubMed: 12813131]

(27). Dhaini HR; Thomas DG; Giordano TJ; Johnson TD; Biermann JS; Leu K; Hollenberg PF; Baker LH Cytochrome P450 CYP3A4/5 Expression as a Biomarker of Outcome in Osteosarcoma. J. Clin. Oncol 2003, 21 (13), 2481–2485. 10.1200/JCO.2003.06.015. [PubMed: 12829666]

(28). Siegel D; Franklin WA; Ross D Immunohistochemical Detection of NAD(P)H:Quinone Oxidoreductase in Human Lung and Lung Tumors. Clin. Cancer Res 1998, 4 (9), 2065–2070. [PubMed: 9748120]

(29). Yang Y; Zhang Y; Wu Q; Cui X; Lin Z; Liu S; Chen L Clinical Implications of High NQO1 Expression in Breast Cancers. J. Exp. Clin. Cancer Res 2014, 33, 14 10.1186/1756-9966-33-14. [PubMed: 24499631]

(30). McFadyen MC; Cruickshank ME; Miller ID; McLeod HL; Melvin WT; Haites NE; Parkin D; Murray GI Cytochrome P450 CYP1B1 Over-Expression in Primary and Metastatic Ovarian Cancer. Br. J. Cancer 2001, 85 (2), 242–246. 10.1054/bjoc.2001.1907. [PubMed: 11461084]

(31). Ma Y; Kong J; Yan G; Ren X; Jin D; Jin T; Lin L; Lin Z NQO1 Overexpression Is Associated with Poor Prognosis in Squamous Cell Carcinoma of the Uterine Cervix. BMC Cancer 2014, 14, 414 10.1186/1471-2407-14-414. [PubMed: 24912939]

(32). Oh E-T; Kim J; Kim JM; Kim SJ; Lee J-S; Hong S-S; Goodwin J; Ruthenborg RJ; Jung MG; Lee H-J; et al. NQO1 Inhibits Proteasome-Mediated Degradation of HIF-1α. Nat Commun 2016, 7 (1), 13593 10.1038/ncomms13593. [PubMed: 27966538]

(33). Hammerich O Reduction of Nitro Compounds and Related Substrates. In Organic electrochemistry; CRC Press: Boca Raton, FL, 2016.

(34). Hettie KS; Klockow JL; Glass TE; Chin FT Near-Infrared Fluorescent Rosol Dye Tailored toward Lymphatic Mapping Applications. Anal. Chem 2019, 91 (4), 3110–3117. 10.1021/acs.analchem.8b05709. [PubMed: 30669835]

(35). Hettie KS; Glass TE Coumarin-3-Aldehyde as a Scaffold for the Design of Tunable PET-Modulated Fluorescent Sensors for Neurotransmitters. Chemistry – A European Journal 2014, 20 (52), 17488–17499. 10.1002/chem.201403128.

(36). Hettie KS; Glass TE Turn-On Near-Infrared Fluorescent Sensor for Selectively Imaging Serotonin. ACS Chem Neurosci 2016, 7 (1), 21–25. 10.1021/acschemneuro.5b00235. [PubMed: 26521705]

(37). Hettie KS; Liu X; Gillis KD; Glass TE Selective Catecholamine Recognition with NeuroSensor 521: A Fluorescent Sensor for the Visualization of Norepinephrine in Fixed and Live Cells. ACS Chem. Neurosci 2013, 4 (6), 918–923. 10.1021/cn300227m. [PubMed: 23527575]

(38). Ofori LO; Withana NP; Prestwood TR; Verdoes M; Brady JJ; Winslow MM; Sorger J; Bogyo M Design of Protease Activated Optical Contrast Agents That Exploit a Latent Lysosomotropic Effect for Use in Fluorescence-Guided Surgery. ACS Chem Biol 2015, 10 (9), 1977–1988. 10.1021/acschembio.5b00205. [PubMed: 26039341]

(39). Tian Z; Tian B; Zhang J Synthesis and Characterization of New Rhodamine Dyes with Large Stokes Shift. Dyes and Pigments 2013, 99 (3), 1132–1136. 10.1016/j.dyepig.2013.06.013.

(40). Jagtap AR; Satam VS; Rajule RN; Kanetkar VR The Synthesis and Characterization of Novel Coumarin Dyes Derived from 1,4-Diethyl-1,2,3,4-Tetrahydro-7-Hydroxyquinoxalin-6-Carboxaldehyde. Dyes and Pigments 2009, 1 (82), 84–89. 10.1016/j.dyepig.2008.11.007.

(41). Stiborova M; Levova K; Barta F; Dracinska H; Sulc M; Hodek P; Frei E; Arlt VM; Schmeiser HH Dicoumarol Inhibits Rat NAD(P)H:Quinone Oxidoreductase in Vitro and Induces Its Expression in Vivo. Neuro Endocrinol. Lett 2014, 35 Suppl 2, 123–132.

(42). Koder RL; Miller AF Steady-State Kinetic Mechanism, Stereospecificity, Substrate and Inhibitor Specificity of Enterobacter Cloacae Nitroreductase. Biochim. Biophys. Acta 1998, 1387 (1–2), 395–405. [PubMed: 9748656]

(43). Liu F; Wang Z; Wang W; Luo J-G; Kong L Red-Emitting Fluorescent Probe for Detection of γ-Glutamyltranspeptidase and Its Application of Real-Time Imaging under Oxidative Stress in Cells and in Vivo. Anal. Chem 2018, 90 (12), 7467–7473. 10.1021/acs.analchem.8b00994. [PubMed: 29785851]

(44). Chen H; Lin W; Cui H; Jiang W Development of Unique Xanthene–Cyanine Fused Near-Infrared Fluorescent Fluorophores with Superior Chemical Stability for Biological Fluorescence Imaging. Chemistry – A European Journal 2015, 21 (2), 733–745. 10.1002/chem.201404718.

(45). Azhdarinia A; Wilganowski N; Robinson H; Ghosh P; Kwon S; Lazard ZW; Davis AR; Olmsted-Davis E; Sevick-Muraca EM Characterization of Chemical, Radiochemical and Optical Properties of a Dual-Labeled MMP-9 Targeting Peptide. Bioorganic & Medicinal Chemistry 2011, 19 (12), 3769–3776. 10.1016/j.bmc.2011.04.054. [PubMed: 21612930]

(46). Shortwave Infrared Fluorescence Imaging with the Clinically Approved Near-Infrared Dye Indocyanine Green | bioRxiv https://www.biorxiv.org/content/10.1101/100768v1 (accessed Oct 26, 2019).

(47). Pastorekova S; Supuran CT Carbonic Anhydrase IX: From Biology to Therapy In Hypoxia and Cancer; Cancer Drug Discovery and Development; Springer, New York, NY, 2014; pp 121–153. 10.1007/978-1-4614-9167-5_6.

(48). Takacova M; Bartosova M; Skvarkova L; Zatovicova M; Vidlickova I; Csaderova L; Barathova M; Breza J; Bujdak P; Pastorek J; et al. Carbonic Anhydrase IX Is a Clinically Significant Tissue and Serum Biomarker Associated with Renal Cell Carcinoma. Oncol Lett 2013, 5 (1), 191–197. 10.3892/ol.2012.1001. [PubMed: 23255918]

(49). Luong-Player A; Liu H; Wang HL; Lin F Immunohistochemical Reevaluation of Carbonic Anhydrase IX (CA IX) Expression in Tumors and Normal Tissues. Am. J. Clin. Pathol 2014, 141 (2), 219–225. 10.1309/AJCPVJDS28KNYZLD. [PubMed: 24436269]

(50). Erpolat OP; Gocun PU; Akmansu M; Ozgun G; Akyol G Hypoxia-Related Molecules HIF-1α, CA9, and Osteopontin : Predictors of Survival in Patients with High-Grade Glioma. Strahlenther Onkol 2013, 189 (2), 147–154. 10.1007/s00066-012-0262-5. [PubMed: 23263636]

(51). Bello RI; Gómez-Dıáz C; Navarro F; Alcaıń FJ; Villalba JM Expression of NAD(P)H:Quinone Oxidoreductase 1 in HeLa Cells ROLE OF HYDROGEN PEROXIDE AND GROWTH PHASE. J. Biol. Chem 2001, 276 (48), 44379–44384. 10.1074/jbc.M107168200. [PubMed: 11567026]

(52). Caballero A; Lázaro JJ; Ramos JL; Esteve-Núñez A PnrA, a New Nitroreductase-Family Enzyme in the TNT-Degrading Strain Pseudomonas Putida JLR11. Environ. Microbiol 2005, 7 (8), 1211–1219. 10.1111/j.1462-2920.2005.00801.x. [PubMed: 16011758]

(53). Hall BS; Wu X; Hu L; Wilkinson SR Exploiting the Drug-Activating Properties of a Novel Trypanosomal Nitroreductase. Antimicrob. Agents Chemother 2010, 54 (3), 1193–1199. 10.1128/AAC.01213-09. [PubMed: 20028822]

(54). Siegel D; Ross D Immunodetection of NAD(P)H:Quinone Oxidoreductase 1 (NQO1) in Human Tissues. Free Radic. Biol. Med 2000, 29 (3–4), 246–253. [PubMed: 11035253]

(55). Yu LJ; Matias J; Scudiero DA; Hite KM; Monks A; Sausville EA; Waxman DJ P450 Enzyme Expression Patterns in the NCI Human Tumor Cell Line Panel. Drug Metab. Dispos 2001, 29 (3), 304–312. [PubMed: 11181500]

(56). Ofori LO; Withana NP; Prestwood TR; Verdoes M; Brady JJ; Winslow MM; Sorger J; Bogyo M Design of Protease Activated Optical Contrast Agents That Exploit a Latent Lysosomotropic Effect for Use in Fluorescence-Guided Surgery. ACS Chem Biol 2015, 10 (9), 1977–1988. 10.1021/acschembio.5b00205. [PubMed: 26039341]

Highlights

- Rational design aids the development of a novel near-infrared molecular probe, NO_2-Rosol
- NO_2-Rosol fluorescence turns ‘on’ in hypoxic environments due to low oxygen concentration and nitroreductase activity
- Lysosomal trapping results in a concentrated, high-contrast, signal in hypoxic cells
- NO_2-Rosol provides a 12-fold fluorescence enhancement to hypoxic over normoxic cells
- The fluorescence signal is stable and unperturbed by constant irradiation, redox-active analytes, or oxidoreductase enzymes
- Initial evaluation suggests NO_2-Rosol would provide high contrast and stable fluorescence for future *in vivo* studies

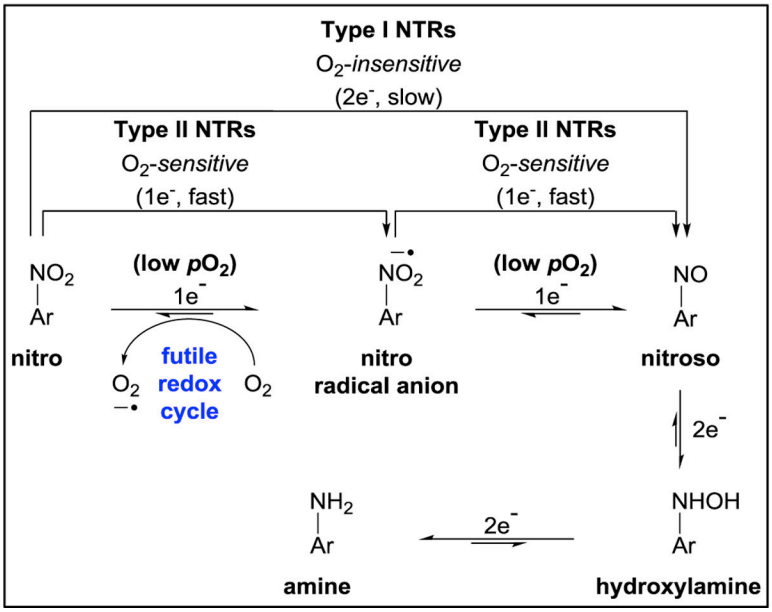

Figure 1. Generalized biological pathways in the reduction of the nitro group of nitroaromatics facilitated by NTRs.

The reductive pathway of each type of NTR, whose enzymatic activity facilitates the reduction of the nitro group of nitroaromatics to the corresponding amine group via producing a nitrosoaromatic intermediate.[33] Type I NTRs facilitate the reduction of the nitro group of nitroaromatics via an oxygen-*insensitive* process that entails the transfer of electrons only in pairs ($2e^-$) from NADPH for producing the nitrosoaromatic intermediate. Type II NTRs facilitate the reduction of the nitro group of nitroaromatics through an oxygen-*sensitive* process that entails successive transfer of only one electron ($1e^-$) from NADPH for sequentially producing the nitro radical anion and the nitrosoaromatic intermediates.

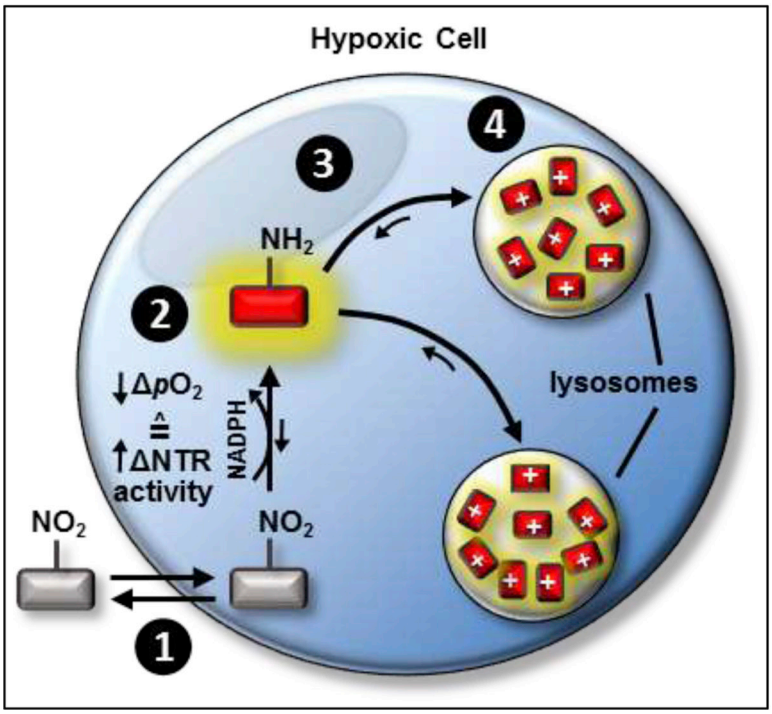

Figure 2. Envisaged operational process of the proposed activatable ultracompact xanthene-core based molecular probe that demonstrates an OFF-ON NIR fluorescence response facilitated via NTR activity.

A low pO_2 environment corresponds to upregulated NTR activity. Step 1: The proposed NTR-selective activatable xanthene core-based molecular probe would diffuse across the cell membrane due to having a neutral net charge. Step 2: The hypoxia-induced (i) upregulated NTR activity in combination with (ii) suppressed oxidation back-reaction of its futile redox cycle would activate and maintain, respectively, its OFF-ON NIR fluorescence response by discontinuing and precluding a d-PeT fluorescence-quenching process from occurring. Step 3: The local equilibrium gradient would result in the activated molecular probe readily diffusing into lysosomes, wherein it would become trapped upon its fluorogenic scaffold assuming a positive net charge due to its integrated THQ moiety becoming weakly-protonated when in lysosomes. On doing so, the activated molecular probe would be permanently retained within the lysosomes. Step 4: The local equilibrium gradient would shift towards additional activated molecular probe localizing to the lysosomes, wherein it too would become similarly protonated and subsequently retained. This strategy would drive the retention of increasing amounts of activated probe, and thereby would help afford enhanced contrast levels due to the signal amplification resulting from such extensive activated molecular probe accumulation within the lysosomes. Ar = aromatic group, NTR = nitroreductase enzyme. pO_2 = partial pressure of oxygen.

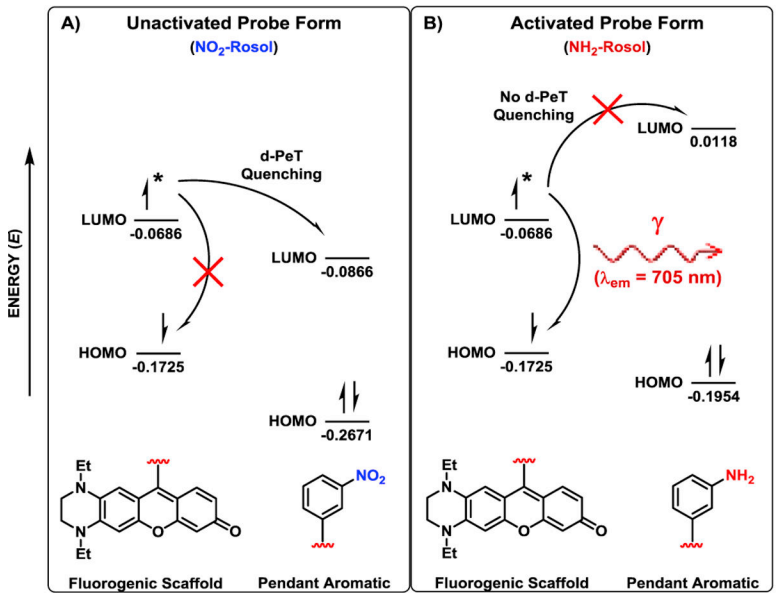

Figure 3. Frontier molecular orbital energy diagram describing the photophysical processes affording NO_2-Rosol an OFF-ON NIR fluorescence response upon its NTR activity-facilitated bioreductive activation.

A) *Favorable* energetics between the LUMO of the fluorogenic scaffold and the LUMO of the pendant *m*-nitrobenzene permit the excited electron that momentarily occupies the LUMO of the former to undergo an intramolecular d-PeT to the LUMO of the latter, and thereby quenches the NIR fluorescence emission that the excited electron would otherwise afford via it subsequently relaxing from the LUMO of the pendant *m*-nitrobenzene in a non-radiative decay process. B) *Unfavorable* energetics between the LUMO of the fluorogenic scaffold and the LUMO of the pendant *m*-aminobenzene precludes a d-PeT fluorescence-quenching process from transpiring between the components, and thereby the excited electron momentarily occupying the LUMO of the fluorogenic scaffold can provide NIR fluorescence emission by relaxing back to the HOMO of the fluorogenic scaffold in a radiative decay process. LUMO = lowest unoccupied molecular orbital, HOMO = highest occupied molecular orbital. Asterisk (*) signifies that an electron from the HOMO of the fluorogenic scaffold exists in an excited electronic state in transitioning to the corresponding LUMO following upon photoexcitation. Molecular orbital energy values are provided in hartrees.

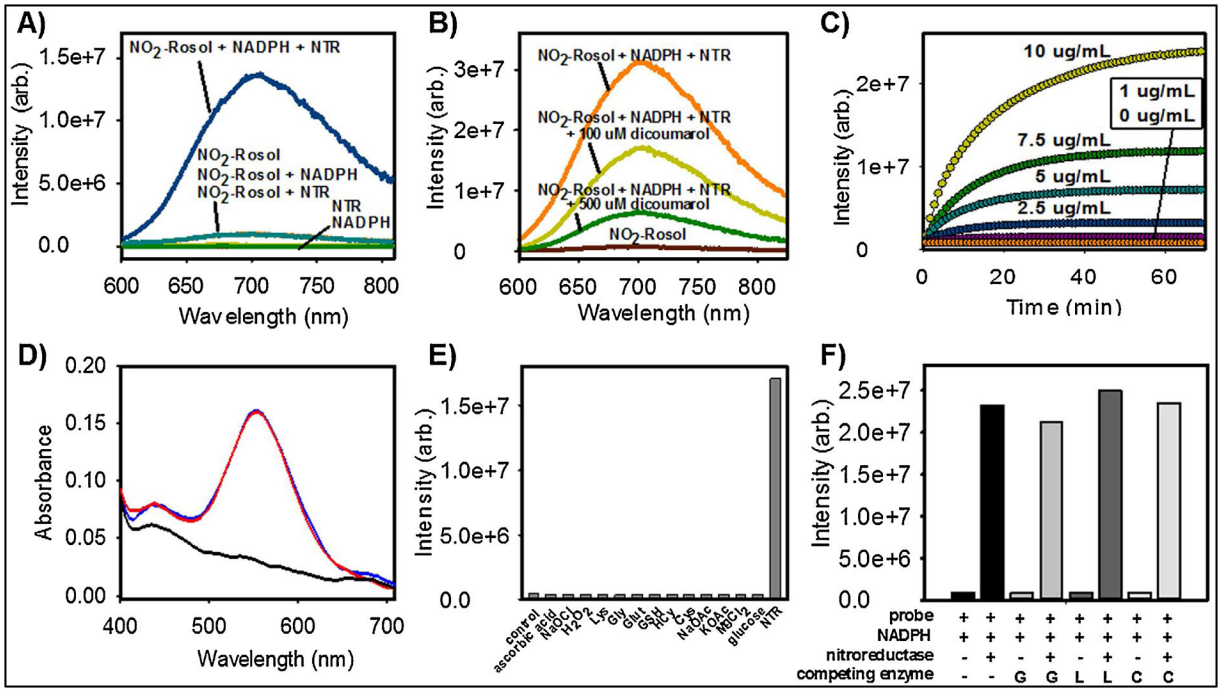

Figure 4. Evaluation of the Photophysical, Spectroscopic, and Selectivity Properties of NO_2-Rosol.

A) Fluorescence activation of **NO_2-Rosol** (20 μM) with and without NTR (10 μg/mL) and/or NADPH (500 μM) in 95:5 PBS:DMSO (λ_{ex} = 550 nm); B) Fluorescence intensity of **NO_2-Rosol** (20 μM) with and without NTR that had been pre-treated with various concentrations of a standard NTR inhibitor (dicoumarol) in the presence of NADPH (500 μM); C) Measurement of the fluorescence intensity of **NO_2-Rosol** upon its activation using various concentrations of NTR (0–10 μg/mL) and a constant concentration of NADPH (500 μM); D) Normalized absorption spectrum of NADPH separately (black) and with **NO_2-Rosol** both before (blue) and 60 min after (red) the addition of NTR (10 μg/mL); E) Fluorescence intensity of **NO_2-Rosol** in the presence of NTR (10 μg/mL) and other biologically-relevant small molecules, all of which are in the presence of NADPH (500 μM): H_2O_2, NaOCl (100 μM each); Cys, HCys, GSH, Glut, Lys, ascorbic acid, Gly (1 mM each); MgCl2 (2 mM); KOAc, NaOAc (50 mM each); F) Competition assay involving **NO_2-Rosol** with and without NTR and/or other biologically-relevant enzymes (10 μg/mL), wherein each arrangement includes the presence of NADPH (500 μM). Lys = lysine, Gly = glycine, Glut = glutamate, GSH = glutathione (reduced form), HCys = homocysteine, Cys = Cysteine, G = glutathione reductase, L = leucine dehydrogenase, C = Cytochrome *c* reductase. Practical considerations required the use of a Type I NTR in performing all solution studies.

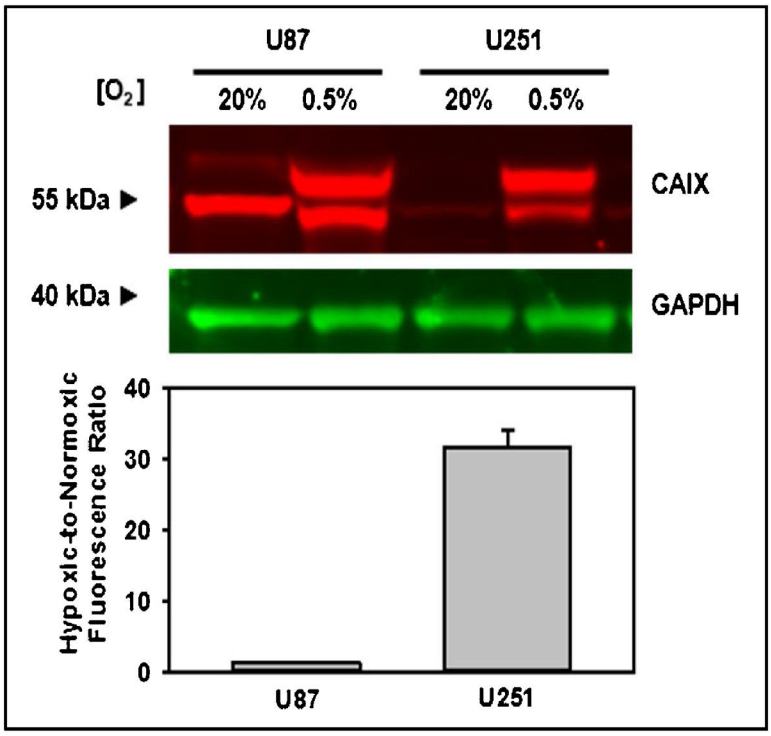

Figure 5. Analysis of hypoxia marker CAIX in glioblastoma cell lysates.

Western blot and semi-quantification of the endogenous hypoxia marker, CAIX, using GAPDH as a loading control in the glioblastoma (GBM) cell lines U87 and U251. Error bars represent the standard error of the mean. CAIX = carbonic anhydrase IX; GAPDH = glyceraldehyde 3-phosphate dehydrogenase.

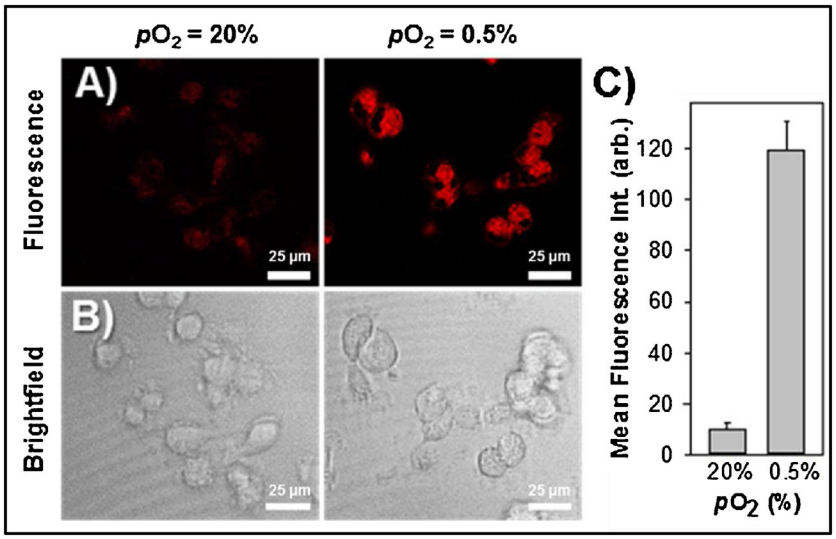

Figure 6. Evaluation of NO_2-Rosol in live cells under normoxic and hypoxic conditions.

Confocal fluorescence microscopy of **NO_2-Rosol** (10 μM) in U251 cells incubated under normoxic (pO_2 = 20%) and hypoxic (pO_2 = 0.5%) conditions. A) Fluorescence imaging (top panels). Emission was collected from 650–800 nm (λ_{ex} = 550 nm). B) Brightfield imaging (bottom panels). Scale bar = 25 μm. C) Quantitative analysis of the mean cell fluorescence intensity. N = 50, $P < 0.0001$

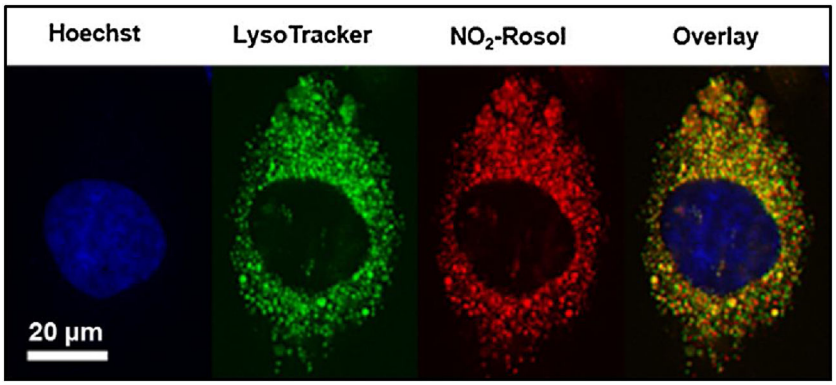

Figure 7. Localization of NO_2-Rosol in live cells under hypoxic conditions upon its activation via upregulated NTR activity.

Confocal fluorescence microscopy of U251 cells under hypoxic conditions incubated with Hoechst 33342 (0.5 μM), LysoTracker Green DND-26 (5 μM), and **NO_2-Rosol** (5 μM). A single cell is shown here. The overlay of the separate corresponding images that utilizes each organelle homing-dye and **NO_2-Rosol** appears to demonstrate significant overlap between LysoTracker Green DND-26 and **NO_2-Rosol**, which was supported by the calculated strong Pearson correlation coefficient of 0.95. Scale bar = 20 μm.

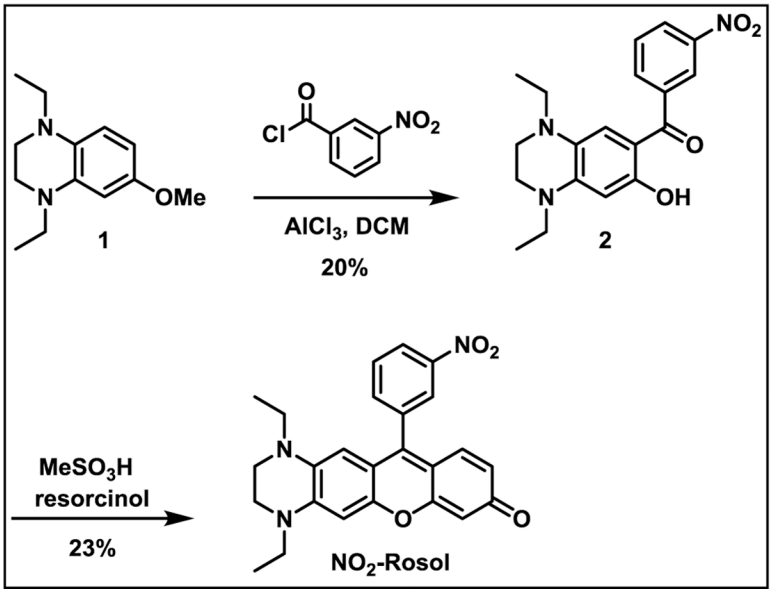

Scheme 1.
Synthesis of NO_2-Rosol.

Table 1.

Spectroscopic and photophysical properties of the unactivated and activated form of NO_2-Rosol.

Compound	λ_{abs} (nm)[a]	λ_{em} (nm)[b]	ε ($M^{-1}cm^{-1}$)	Φ_{fl}[c]	Brightness ($M^{-1}cm^{-1}$)
NO_2-Rosol (unactivated form)	550	710	11,000	0.0005	5.5
NH_2-Rosol (activated form)	548	705	10,300	0.0205	210

[a] Measured maximum absorption wavelength of each compound in buffer;

[b] Measured maximum fluorescence emission wavelength of each compound upon photoexcitation at its respective λ_{abs} in buffer.

[c] Φ_{fl} is the measured relative fluorescence quanum yield using erythrosine B in buffer as a reference (Φ_{fl} = 0.02).